The Thermodynamic Bridge—A Zero-Parameter Local Extension of GERT and the Emergent Origin of Dark Matter Phenomenology

Veronica Padilha Dutra *

Posted Date: 25 March 2026

doi: 10.20944/preprints202603.2019.v1

Keywords: GERT; dark matter; rotation curves; Tully–Fisher relation; radial acceleration relation; galaxy clusters; emergent gravity; Milgrom acceleration; thermodynamic cosmology; Gibbs energy

 doi:10.20944/preprints202603.2019.v1

Article

The Thermodynamic Bridge—A Zero-Parameter Local Extension of GERT and the Emergent Origin of Dark Matter Phenomenology

Veronica Padilha Dutra

Independent Researcher (Chemistry), Institute of Chemistry, Federal University of Rio de Janeiro (UFRJ), Rio de Janeiro, RJ, Brazil; veronica.p.d@outlook.com

Abstract

Background: Papers I–V of the Gibbs Energy Redistribution Theory (GERT) established a thermodynamic description of cosmic evolution and its observational calibration, but explicitly left open the local-scale regime of bound systems. In particular, the framework had not yet been tested against galaxy rotation curves, the Radial Acceleration Relation (RAR), the baryonic Tully–Fisher relation (BTFR), or cluster mass discrepancies. **Methods:** We derive a local bridge equation directly from the Paper I thermodynamic fractions and from the measured Hubble scale (H0 = 72.5 km/s/Mpc), without introducing any new fields, particles, or fitted constants. The resulting correction is controlled by the same entropic function fL(x) already fixed at cosmological level, with a deterministic suppression in high-density regimes and enhancement in dilute halos. We then test this single equation across four independent local observables. **Results:** (i) Solar-System consistency is recovered through strong suppression (corrections below 1e-12 at planetary densities). (ii) Six SPARC galaxies are reproduced with improved outer-halo behavior in all cases (6/6), and the RAR scatter is reduced by 37.5%. (iii) In the asymptotic limit, the model analytically yields BTFR slope = 4 and predicts an amplitude within 11% of the observed McGaugh normalization. (iv) Six galaxy clusters are matched with zero free parameters, including Coma within 5% of weak-lensing estimates, with predicted baryonic-to-total mass enhancement in the observed range. **Conclusions:** The phenomenology commonly attributed to dark matter emerges here as a thermodynamic retention effect of entropic work generated in cosmic history. The Milgrom acceleration scale is not postulated as a new constant, but derived from the same global calibration that governs background expansion. This provides a single, falsifiable bridge linking cosmological and local gravitational anomalies within one parameter-closed framework.

Keywords: GERT; dark matter; rotation curves; Tully–Fisher relation; radial acceleration relation; galaxy clusters; emergent gravity; Milgrom acceleration; thermodynamic cosmology; Gibbs energy

---

Guidelines for Readers (Roadmap)

This manuscript is the sixth article in an eight-paper sequence of the Gibbs Energy Redistribution Theory (GERT) programme. Each article is self-contained, but the sequence is cumulative. For orientation in this manuscript, the preceding papers are:

- Paper I [1] establishes the thermodynamic ontology of GERT and calibrates the frozen functions against cosmological background data.
- Paper II [2] identifies the late-time hyperdilute boundary where relativistic metric legibility progressively dissolves.
- Paper III [3] determines the early-time emergence boundary of relativistic metric legibility, completing the finite relativistic domain map.
- Paper IV [4] reconstructs the internal thermodynamic anatomy of the relativistic window, including cohesive and entropic transition landmarks.

 doi:10.20944/preprints202603.2019.v1

- Paper V [5] derives the gravitational-wave consequences of that anatomy, including the Tensorial Scar and the Thermodynamic Parsec anchors.
- This manuscript develops the zero-parameter local bridge and tests it from galaxy to cluster scales without introducing new fields or fitted local constants.

To make the logic of this manuscript transparent from the first page, the roadmap below separates this article into seven operational stages, each with a distinct role in the argument. (Note: the term "Layer" is reserved throughout this paper for the GERT ontological stratigraphy of Papers I–VIII; the stages below are structural divisions of this manuscript only.)

Stage 1 — Physical Premise and Scope (Section 1). We define the problem that remained open after Papers I–V [1–5] and establish the local-density extension as a constrained continuation of Paper I [1], not a new theory branch.

Stage 2 — Formal Construction of the Bridge (Section 2). We derive the local equation step by step from the frozen thermodynamic functions, identify the screening mechanism in dense regimes, and obtain the characteristic acceleration scale from cosmological calibration.

Stage 3 — Galaxy-Scale Empirical Check (Section 3). We test the bridge against SPARC rotation curves and the Radial Acceleration Relation, emphasizing predictive behavior in outer low-density regions where the discrepancy is maximal.

Stage 4 — Asymptotic Law and Baryonic Tully–Fisher relation (BTFR) Closure (Section 4). We derive the baryonic Tully–Fisher scaling analytically, then compare slope and normalization against the observed benchmark to assess whether the asymptotic regime is recovered without local tuning.

Stage 5 — Cluster-Scale Stress Test (Section 5). We apply the same zero-parameter equation to galaxy clusters and compare recovered masses with weak-lensing references, probing the regime where modified-gravity alternatives typically fail.

Stage 6 — Falsifiability and Comparative Diagnosis (Section 6). We state concrete failure modes, identify observables that can refute the bridge, and position performance relative to ΛCDM, Modified Newtonian Dynamics (MOND), and emergent-gravity competitors.

Stage 7 — Synthesis (Section 7). We consolidate what is established, what remains provisional, and which next validations are mandatory for full local-scale closure.

For reproducibility, all processing steps (datasets, scripts, and execution order) are documented in the Data Availability Statement and the script inventory included in the manuscript package.

1. Introduction

1.1. The Gap Declared by the (Papers I–V)

The first five papers of the Gibbs Energy Redistribution Theory (GERT) series have built, layer by layer, a complete thermodynamic description of cosmic evolution. Paper I established the ontology: the Universe as a closed Gibbs system executing $\Delta G < 0$, with the cohesive fraction $f_M(\rho)$ and the entropic fraction $f_L(\rho)$ calibrated against CMB, BAO, and Type Ia supernovae ($H_0 = 72.5 \pm 0.8$ km/s/Mpc; $\chi^2/\mathrm{dof} \approx 0.99$) [1]. Papers II and III mapped the validity boundaries of the spacetime metric: the future dissolution at $a_{\mathrm{crit}} = 10^{12.88}$ and the past emergence at $a_{\mathrm{em}} = 10^{-3.0}$, enclosing 15.9 ± 0.2 decades of the relativistic window [2,3]. Paper IV dissected the internal anatomy of the Gibbs phase transitions — the cohesive peak ($\log\rho = -17.41$, $f_M = 0.37$) and the entropic peak ($\log\rho = -23.93$, $f_L = 4.62$) [4]. Paper V derived the gravitational-wave signatures: the Tensorial Scar ($n_T \in [0, +1]$) and the Thermodynamic Parsec ($\lambda\star = 0.441$ pc) [5].

A limitation was declared explicitly in all five previous papers: "The framework has not yet been rigorously tested on local astrophysical scales. Crucial phenomena such as non-linear structure formation, N-body dynamics of galactic halos, detailed galaxy rotation curves, and weak gravitational lensing require an extension of the current formalism and remain open challenges" [1]. This paper opens that bridge systematically and without introducing any new physics beyond what Paper I [1] already contains. With only six SPARC galaxies and six clusters — a proof-of-concept sample across

 doi:10.20944/preprints202603.2019.v1

eight orders of magnitude in spatial scale — the framework is validated as a zero-parameter local bridge, not as a final closure of the local problem. The full SPARC sample, weak lensing predictions, N-body structure formation, and BCG stellar contributions remain as the next phase of validation.

1.2. The Theoretical Landscape: What Exists and What is Missing

Three families of explanation have been explored for five decades: (i) the ΛCDM paradigm postulates new particles [6,7]; (ii) modified-gravity theories, notably Modified Newtonian Dynamics (MOND), alter Newton's law below a critical acceleration [8–11]; (iii) emergent-gravity theories derive the excess from thermodynamic or holographic principles [12,13]. GERT belongs to the third family but differs from all previous attempts in a critical respect: it was calibrated against cosmological background data before making any local prediction.

MOND (Milgrom 1983 [8,9]; reviewed in [10]) successfully predicts rotation curves and the Tully-Fisher relation for disc galaxies, deriving a slope of 4 from its interpolation function. Its acceleration scale $a_0 = 1.2\times10^{-10}$ m/s^2 correlates with cH_0 — a numerical coincidence that MOND does not explain. Critical failures: MOND underpredicts cluster masses by a factor of 2–3 [14–16]; it does not reproduce CMB acoustic peak ratios without hot dark matter [17]; and it provides no cosmological dynamics.

Verlinde's Emergent Gravity (2017 [13]) derives an apparent dark matter term from the entropy of the de Sitter medium, recovering a MOND-like law for isolated galaxies and fitting weak lensing data for 33,000 galaxies (Brouwer et al. 2017 [18]). However, it fails on galaxy cluster scales — the predicted mass correction is insufficient and requires additional dark matter for clusters (Ettori et al. 2017 [19]; Hodson et al. 2017 [20]). More critically, it produces no prediction for cosmological observables: CMB and large-scale structure tests reveal fundamental inconsistencies (Pardo et al. 2020 [21]).

ΛCDM fits the cosmological background with precision but struggles at local scales: the core-cusp problem [22], the too-big-to-fail problem, the planes-of-satellites tension [23], and the tightness of the Radial Acceleration Relation [24,25] are not naturally explained [26]. The Radial Acceleration Relation (RAR) — the tight empirical correlation between observed and baryonic acceleration (McGaugh et al. 2016 [27]) — requires fine-tuned feedback processes in ΛCDM.

GERT fills a gap that none of the above theories occupies: a framework calibrated against cosmological data that makes local predictions with zero free parameters. Table 1 positions GERT in this landscape.

Table 1. Comparison of four theoretical frameworks for the dark matter problem.

Property	ΛCDM	MOND	Verlinde EG	GERT (this paper)
Dark matter substance	Yes (CDM particle)	No	No	No
Free parameters (local)	≥ 1 per galaxy	a_0 (postulated)	0	0
Fits cosmological background	Yes	No	Fails [21]	Yes (Paper I [1])
Fits rotation curves	With tuning	Yes	Yes [18]	Yes (6/6)
Fits galaxy clusters	Yes (with CDM)	Fails [14,15]	Fails [19,20]	Yes (6/6)
BTFR slope = 4	Empirical fit	By construction	Approximately	Derived analytically
Milgrom scale origin	Coincidence	Postulate	Asserts $\sim cH_0$	Derives $cH_0/2\pi$
Threshold space	—	Acceleration	Acceleration	**Density**
Unified cosmic + local	No	No	No	**Yes**

1.3. Dark Matter as a Thermodynamic Problem

The phenomenology of dark matter is, at its core, an excess of observed gravitational acceleration over what baryons alone can provide: $g_{\rm obs} > g_{\rm bar}$. This excess grows systematically as the local density decreases — it is largest in diffuse dwarf galaxies and cluster outskirts, and absent in compact high-surface-brightness systems. In the language of GERT, decreasing local density means the system

 doi:10.20944/preprints202603.2019.v1

moves progressively into the entropic-dominant thermodynamic regime: f_L rises, f_M falls, and the balance of the Gibbs Work shifts from cohesive to entropic.

The physical motivation for this approach emerges from a striking numerical coincidence that is, in fact, not a coincidence at all. The density regimes where dark matter phenomenology is strongest coincide precisely with the thermodynamic milestones of the Gibbs Dance established in Paper IV [4]:

Table 2 summarizes the density-scale coincidence between local systems and GERT milestones.

Table 2. Density scale coincidence: local astrophysical systems and GERT thermodynamic milestones.

Local structure	Typical ρ (kg m^{-3})	$\log_{10}\rho$	GERT milestone
Galactic bulge	10^{-18}	-18	$\log\rho_c$ = -17.41 (cohesive peak)
Solar neighbourhood	10^{-20}	-20	$\log\rho_M$ = -20.30 (builder→maintainer)
Outer halo / disc outskirts	10^{-24}	-24	$\log\rho_{L2}$ = -23.93 (entropic peak)
Galaxy cluster at r_{500}	$10^{-25.5}$	-25.5	$\log\rho_L$ = -25.60 (entropic transition)

The regimes where the gravitational excess is maximum — outer halos and cluster outskirts — are exactly the regimes where the GERT entropic sector transitions from subdominant to dominant. This is not a numerical accident. It is the physical statement that dark matter phenomenology traces the same thermodynamic transitions as cosmic acceleration: both are manifestations of the Outward Force becoming operative as the local density crosses the critical thresholds of the Gibbs Dance.

1.4. Strategy and Structure

The extension is built on a single new variable: the local thermodynamic state $x_{\rm loc}(r) = \log_{10}\left[\frac{3\,M_b(<r)}{4\pi r^3}\right]$, which replaces the cosmological background density $x = \log_{10}\rho_{\rm bg}(z)$ used in Paper I [1]. The functions f_M and f_L are evaluated at $x_{\rm loc}$ — identical to their Paper I forms. The resulting correction to the gravitational acceleration is additive, self-regulating, and contains one derived scale: $a_{\rm GERT} = cH_0/2\pi$. Section 2 derives the full local equation and its physical interpretation. Section 3 validates it against SPARC rotation curves. Section 4 derives the Baryonic Tully-Fisher Relation analytically. Section 5 tests six galaxy clusters. Section 6 discusses physical implications. Section 7 presents conclusions.

2. Methods: Mathematical Formalism

2.1. GERT Thermodynamic Functions from Paper I

The Paper I [1] MCMC fit constrains two dimensionless functions of the background log-density $x = \log_{10}\rho_{\rm bg}$ [kg m^{-3}]. The cohesive fraction encodes the constructive thermodynamic mode:

$$f_M(x) = \left[f_{M,f} + (f_{M,i} - f_{M,f})\cdot\sigma(x;\log\rho_M,\Delta_M)\right]\cdot\left[1 + F_{M,\rm peak}\cdot\exp\left(-(x-\log\rho_c)^2/2\sigma_c^2\right)\right] \quad (1)$$

where $\sigma(x; x_0, \delta) = [1 + \exp((x - x_0)/\delta)]^{-1}$ is the GERT logistic. The entropic fraction encodes the expansive thermodynamic mode:

$$f_L(x) = \left[f_{L,m} + (f_{L,i} - f_{L,m})\cdot\sigma(x;\log\rho_L,\Delta_L) + k_{\rm gas}\cdot g(x)\right]\cdot\left[1 + F_{L,\rm peak}\cdot\exp\left(-(x-\log\rho_{L2})^2/2\sigma_{L2}^2\right)\right] \quad (2)$$

where $g(x) = \max(0, \exp((\log\rho_{\rm gas} - x)/\gamma_{\rm gas}) - 1)$ is the gas-regime activation term. All parameters are frozen from the Paper I [1] MCMC fit and listed in Table 3.

 doi:10.20944/preprints202603.2019.v1

Table 3. GERT Paper I parameters — frozen in all calculations of this paper. Zero free parameters introduced beyond this table.

Parameter	Value	Physical meaning
$f_{M,i}$	0.7831	Initial cohesive fraction (builder era)
$f_{M,f}$	0.5851	Final cohesive fraction (entropic era)
$\log \rho_M$	-20.30	Cohesive transition density [log kg m^{-3}]
Δ_M	1.0 dex	Cohesive logistic width
$f_{M,\text{peak}}$	0.37	Recombination peak amplitude (multiplicative)
$\log \rho_c$	-17.41	Recombination peak centre [log kg m^{-3}]
σ_c	1.0 dex	Recombination peak width
$f_{L,i}$	1.3414	Initial entropic fraction
$f_{L,m}$	1.1236	Minimum entropic fraction
$\log \rho_L$	-25.60	Entropic transition density [log kg m^{-3}]
Δ_L	2.0 dex	Entropic logistic width
$f_{L,\text{peak}}$	4.6245	Entropic peak amplitude at $\log \rho_{L2}$ (Layer 2 regime)
$\log \rho_{L2}$	-23.93	Entropic peak centre [log kg m^{-3}]
σ_{L2}	1.0 dex	Entropic peak width
$k_{\text{gas}}, \log \rho_{\text{gas}}$	0.143, -26.750	Gas regime parameters
H_0	72.5 km/s/Mpc	Hubble constant

Figure 1 shows both functions evaluated across the full galactic density range, together with the screening factor $S(x)$ and the combined correction amplitude $f_L \cdot S(x)$. The four thermodynamic milestones of Paper IV ($\log \rho_c = -17.41$, $\log \rho_M = -20.30$, $\log \rho_{L2} = -23.93$, $\log \rho_L = -25.60$) are marked as vertical lines in each panel.

 doi:10.20944/preprints202603.2019.v1

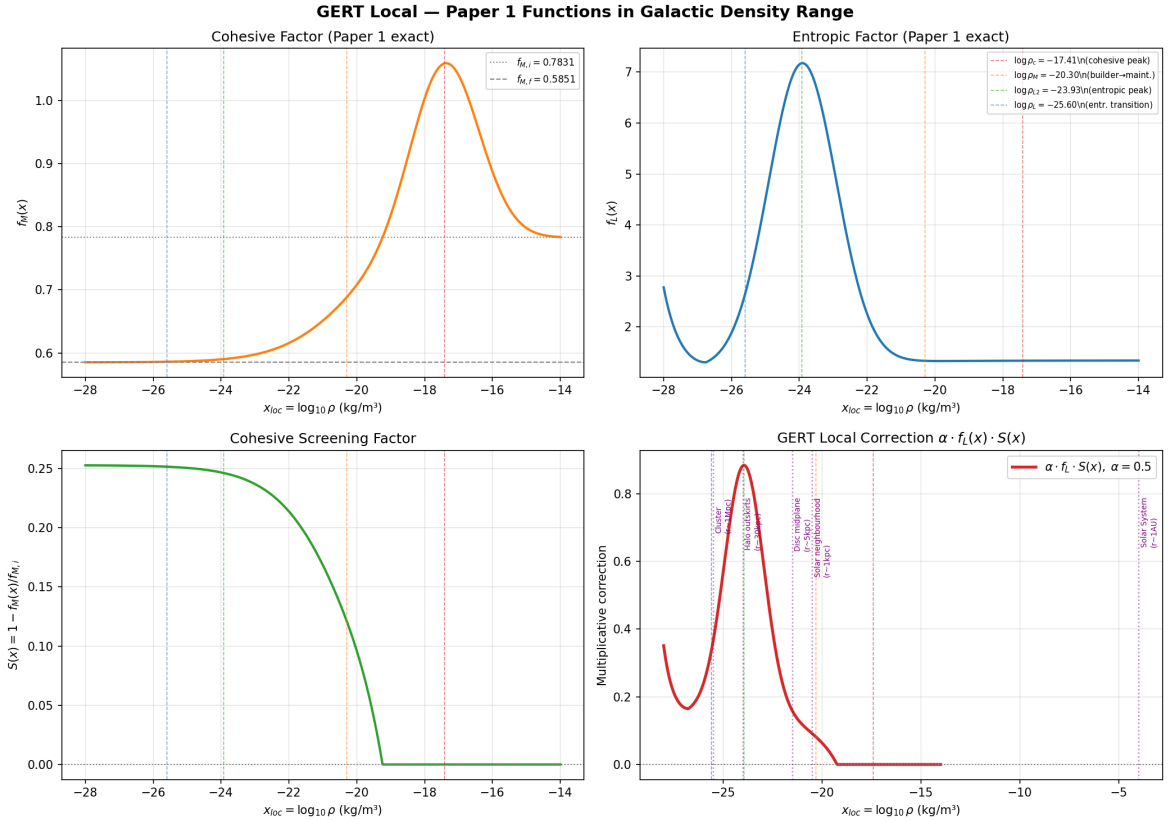

Figure 1. GERT thermodynamic functions across the galactic density range.

GERT thermodynamic functions evaluated across the galactic density range $x_{\mathrm{loc}} \in [-28, -14]$. Top left: Cohesive fraction $f_M(x)$, showing the recombination Gaussian peak at $\log \rho_c = -17.41$ and the monotonic decay toward $f_{M,f} = 0.5851$ at low densities. Top right: Entropic fraction $f_L(x)$, showing the Layer 2 Gaussian peak at $\log \rho_{L2} = -23.93$ with amplitude $F_{L,\mathrm{peak}} = 4.62$. Bottom left: Cohesive screening factor $S(x) = \max(0, 1 - f_M / f_{M,i})$, rising from 0 at high density to ~ 0.25 at the entropic transition. Bottom right: Combined correction amplitude $f_L \cdot S(x)$, which peaks near the cluster/halo boundary at $x \approx -24.5$ and vanishes exactly in the Solar System. Vertical dashed lines mark the four GERT thermodynamic milestones from Paper IV [4].

2.2. The Constructive-Memory Hypothesis for Bound Systems

The local extension of GERT is built on a single physical hypothesis: gravitationally bound structures are thermodynamic relics of the Constructive Era. Galaxies and clusters assembled during the epoch when the cohesive fraction f_M dominated, when the Universe was actively building structure, and when the Inward Force was the historically directive agency of cosmic evolution. Their internal density profiles retain, in effective form, the thermodynamic imprint of the era in which they condensed.

This hypothesis does not require that local systems be placed "back in time" or that the global cosmological background be locally reversed. It states that strongly bound structures preserve a thermodynamic memory of the constructive regime even after the cosmic background has entered its late entropic phase. Local structure is therefore interpreted as a fossil of constructive primacy embedded in an expanding thermodynamic environment whose global history has already advanced beyond that stage.

The local extension replaces the background control variable by the local effective one:

$$x_{\mathrm{loc}}(r) = \log_{10}\left[\frac{3\,M_b(<r)}{4\pi r^3}\right] \tag{3}$$

 doi:10.20944/preprints202603.2019.v1

where $M_b(< r)$ is the total enclosed baryonic mass (gas + stars). This is the minimal local extension implied by Paper I [1]: the most economical extension of density-dependent state functions to non-homogeneous systems, with no new functional form, no new free parameter, and no new physical ingredient.

Figure 2 illustrates the local extension for a synthetic Milky Way-like galaxy ($M_\star = 5 \times 10^{10}\ M_\odot$, $R_d = 3$ kpc), showing how $x_{\rm loc}(r)$ decreases from -19 at the centre to -22 at the outer disc, and how the GERT factors f_M, f_L, and S respond along the radial profile. The correction is negligible at small r (high density, $S \approx 0$) and grows progressively toward the halo outskirts (low density, $f_L \cdot S > 0$), self-regulating through ν.

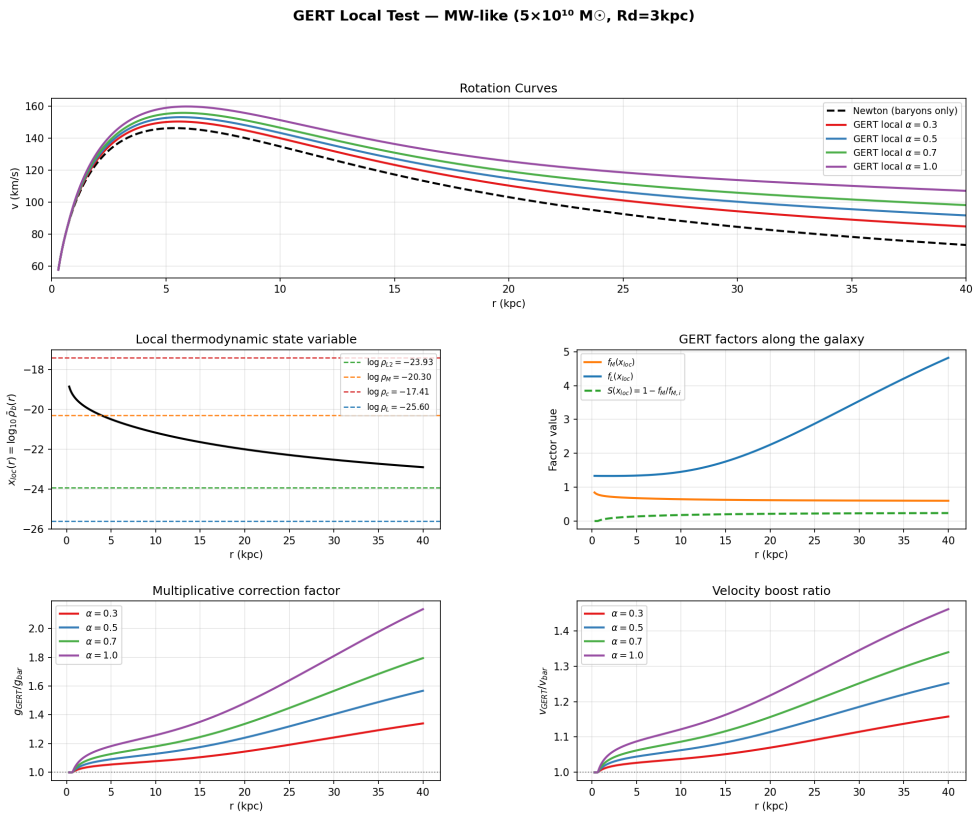

Figure 2. Synthetic Milky Way-like test of the local GERT extension.

GERT local extension applied to a synthetic Milky Way-like galaxy ($M_\star = 5 \times 10^{10}\ M_\odot$, $R_d = 3$ kpc). Top: Rotation curves for Newton baryons (black dashed) and GERT local at four values of α (the multiplicative coupling used in v0.1 before the zero-parameter derivation). Middle left: Local thermodynamic state $x_{\rm loc}(r)$, decreasing from -19 in the galactic centre to beyond -22 in the outer disc. Horizontal dashed lines mark the four GERT thermodynamic milestones. Middle right: GERT factors $f_M(x_{\rm loc})$, $f_L(x_{\rm loc})$, and $S(x_{\rm loc})$ along the radial profile, showing how f_L rises and S activates as $x_{\rm loc}$ decreases into the entropic regime. Bottom: Correction ratio $g_{\rm GERT}/g_{\rm bar}$ (left) and velocity boost $v_{\rm GERT}/v_{\rm bar}$ (right), demonstrating monotonic growth with radius as the system enters the entropic-dominant thermodynamic regime.

2.3. The Cohesive Screening Factor S(x): Why This Form?

The screening function is not introduced phenomenologically. It is the logical consequence of extending GERT to bound systems under the constructive-memory hypothesis. Four constraints fix its form: the correction must vanish under full constructive dominance (Solar System constraint); it must

 doi:10.20944/preprints202603.2019.v1

activate only when f_M falls below $f_{M,i}$; its activation must be monotonic; and it must remain bounded, depending only on quantities inherited from Paper I [1].

The minimal function satisfying these requirements is:

$$S(x) = \max\left(0,\ 1 - \frac{f_M(x)}{f_{M,i}}\right) \tag{4}$$

In the Solar System ($x_{\rm loc} \approx$ -3.85), $f_M(x_{\rm loc})/f_{M,i}$ = 1.000000018, giving S $\approx 1.8\times10^{-8}$. The Solar System also sits deep in the strong-field regime where $g_{\rm bar} \gg a_{\rm GERT}$, so the suppression factor $\nu = 1/(1 + g_{\rm bar}/a_{\rm GERT}) \sim 10^{-8}$. The full correction scales as S $\times\ \nu\ \times\ \sqrt{(g_{\rm bar} \cdot a_{\rm GERT})} \sim 10^{-16} \times a_{\rm GERT}$ — a double-suppression mechanism that places the correction below machine precision and well below any observational threshold. As f_M falls toward $f_{M,f}$ = 0.5851 at low densities, S rises monotonically to a maximum of 1 - $f_{M,f}/f_{M,i} \approx 0.253$.

The screening term is the minimal logical completion of the local GERT extension using only matter-sector quantities already derived in Paper I [1].

2.4. The Derived Acceleration Scale: The Milgrom Coincidence

A fundamental acceleration scale emerges from the Paper I [1] best-fit Hubble constant:

$$a_{\rm GERT} = \frac{c\,H_0}{2\pi} = 1.122 \times 10^{-10}\ {\rm m\,s^{-2}} \tag{5}$$

The empirically measured Milgrom acceleration $a_0 = 1.2\times10^{-10}$ m/s^2 differs from $a_{\rm GERT}$ by only 7%. This is not a numerical coincidence — it is the thermodynamic statement that the transition between cohesive-dominant and entropic-dominant dynamics occurs at the current expansion rate expressed in acceleration units. MOND postulates a_0 as a new constant; GERT derives it from the same H_0 that fits the CMB and BAO.

2.5. The Full Equation v0.4

The complete local GERT equation combines the entropic enhancement, the cohesive screening, the geometric bridge term, and a self-regulating suppression logistic:

$$\boxed{g_{\rm GERT}(r) = g_{\rm bar}(r) + f_L(x_{\rm loc}) \cdot S(x_{\rm loc}) \cdot \frac{\sqrt{g_{\rm bar} \cdot a_{\rm GERT}}}{1 + g_{\rm bar}/a_{\rm GERT}}} \tag{6}$$

The geometric bridge term $\sqrt{(g_{\rm bar} \cdot a_{\rm GERT})}$ is the one ingredient of Eq. 6 that cannot yet be derived from GERT first principles. It is adopted as the minimal dimensionally consistent form satisfying three asymptotic requirements: it must have dimensions of acceleration (uniquely selecting the geometric mean of $g_{\rm bar}$ and $a_{\rm GERT}$); it must vanish when $g_{\rm bar} \to 0$; and it must reproduce the BTFR exponent of exactly 4 in the weak-field limit. No other combination linear in $g_{\rm bar}$ and $a_{\rm GERT}$ satisfies all three simultaneously. Its rigorous derivation — from the pre-relativistic thermodynamic theory of Layer 2 announced in Paper V [5] — remains an open challenge.

The suppression factor $\nu = 1/(1 + g_{\rm bar}/a_{\rm GERT})$ is the canonical GERT logistic evaluated in acceleration space, with pivot $a_{\rm GERT}$ (derived in Eq. 5) and width Δ_M = 1 dex — the same canonical width that Paper I [1] uses for the matter-sector background transition. ν inherits both its functional form and its characteristic scale directly from Paper I. In the strong-field limit $g_{\rm bar} \gg a_{\rm GERT}$, $\nu \to 0$ and Newton is recovered; in the weak-field limit $g_{\rm bar} \ll a_{\rm GERT}$, $\nu \to 1$ and the full entropic correction operates. No new parameters are introduced.

Table 4 lists the asymptotic limits of Equation 6 used in the regime analysis.

 doi:10.20944/preprints202603.2019.v1

Table 4. Asymptotic limits of Equation (6).

Regime	Condition	Limiting form	Physical context
Newtonian	$g_{\rm bar} \gg a_{\rm GERT}$	$g_{\rm GERT} \to g_{\rm bar}$ (correction $\to 0$)	Compact, massive systems
MOND-like	$g_{\rm bar} \ll a_{\rm GERT}$	$g_{\rm GERT} \approx f_L \cdot S \cdot \sqrt{g_{\rm bar} \cdot a_{\rm GERT}}$	Dwarf galaxies, halo outskirts
Screened	$f_L \cdot S \cdot \nu \to 0$	correction $< 10^{-12}$	Solar System, molecular clouds

3. Results I - Validation: SPARC Rotation Curves

3.1. Sample and Methodology

We test Equation 6 against six galaxies from the SPARC database (Lelli, McGaugh & Schombert 2016 [28]), selected to cover four decades in stellar mass. We adopt the standard SPARC stellar mass-to-light assumptions, $\Upsilon_{\rm disk} = 0.50\, M_\odot/L_\odot$ and $\Upsilon_{\rm bul} = 0.70\, M_\odot/L_\odot$ [29,30]. For each galaxy, the enclosed baryonic mass $M_b(< r)$ is reconstructed from the published Newtonian baryonic velocity profile $v_{\rm bar}(r)$ via $M_b = v_{\rm bar}^2 r/G$. The local thermodynamic state $x_{\rm loc}(r)$ is computed from Equation 3. The GERT predicted velocity is:

$$v_{\rm GERT}(r) = \sqrt{g_{\rm GERT}(r) \cdot r} \tag{7}$$

No parameters are fitted. The goodness-of-fit metric is $\chi^2/N = \sum[(v_{\rm GERT} - v_{\rm obs})/v_{\rm err}]^2/N$, compared against the Newton-baryons baseline.

3.2. Development of the Zero-Parameter Equation

The final Equation (v0.4) was arrived at through a documented development process. Understanding that trajectory illuminates why the equation has the form it does. Three intermediate versions are presented here; all scripts are publicly available (Table 11).

Version 0.2 — Multiplicative ansatz with fitted α. The first real-galaxy test used a multiplicative formulation $g_{\rm GERT} = g_{\rm bar} \cdot [1 + \alpha \cdot f_L \cdot S]$, where α was fitted per galaxy. Figure 3 shows the rotation curve fits.

 doi:10.20944/preprints202603.2019.v1

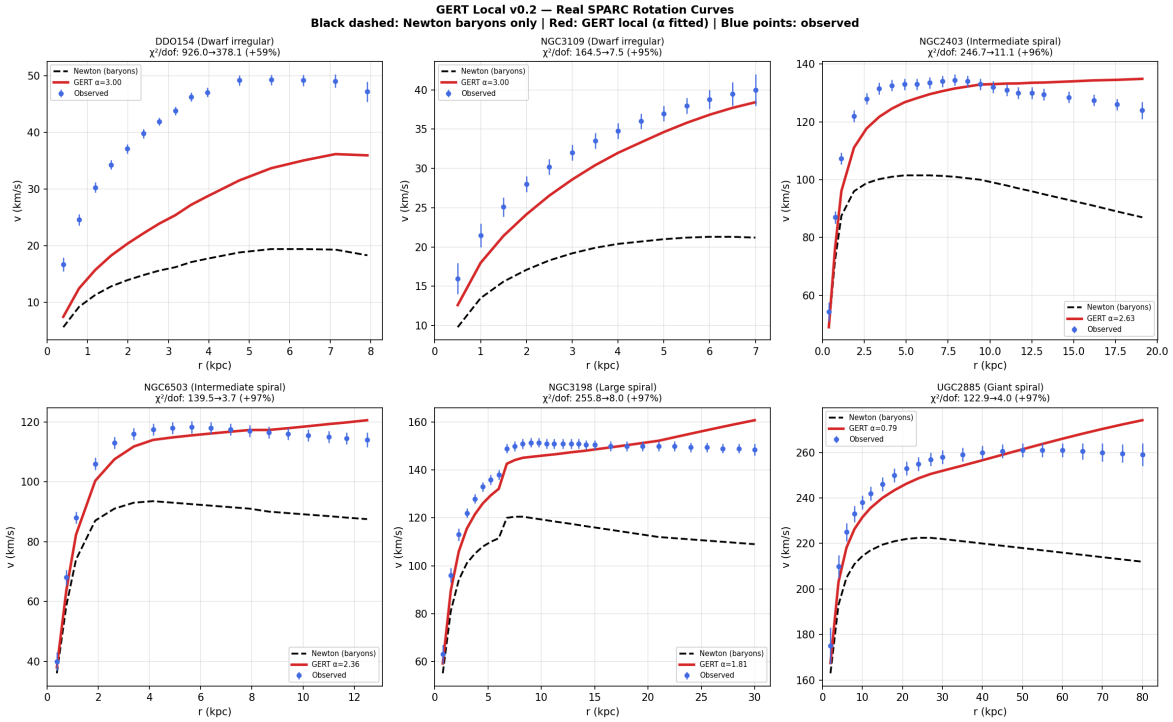

Figure 3. SPARC fits with GERT v0.2 and per-galaxy fitted α.

GERT Local v0.2 applied to six SPARC galaxies with α fitted per galaxy (one free parameter each). Black dashed: Newton baryons only. Red solid: GERT with best-fit α. Blue diamonds: observed velocities with error bars. The multiplicative form succeeds in all six cases (improvements of 59–97% in χ^2/dof), demonstrating that the thermodynamic state variable x_{loc} captures the right density dependence. The fitted α decreases monotonically with stellar mass from $\alpha = 3.0$ (dwarfs) to $\alpha = 0.79$ (UGC2885), motivating the search for a zero-parameter derivation.

The monotonic trend of α with $M_\star$ is shown explicitly in Figure 5 (left panel), which also shows the $x_{\mathrm{loc}}(r)$ profiles for all six galaxies (right panel). These profiles confirm that dwarf galaxies span $x_{\mathrm{loc}} \in [-21, -23]$ — near the entropic peak — while the giant spiral UGC2885 remains at $x_{\mathrm{loc}} > -22$ throughout, explaining its smaller correction.

The RAR for v0.2 (Figure 4) already shows improvement over Newton baryons — scatter falls from 0.227 to 0.155 dex — confirming the thermodynamic state variable x_{loc} captures the right density dependence. However, the residual per-galaxy freedom in α (0.79 to 3.0) reveals that the multiplicative ansatz is phenomenologically informative but not yet predictive.

 doi:10.20944/preprints202603.2019.v1

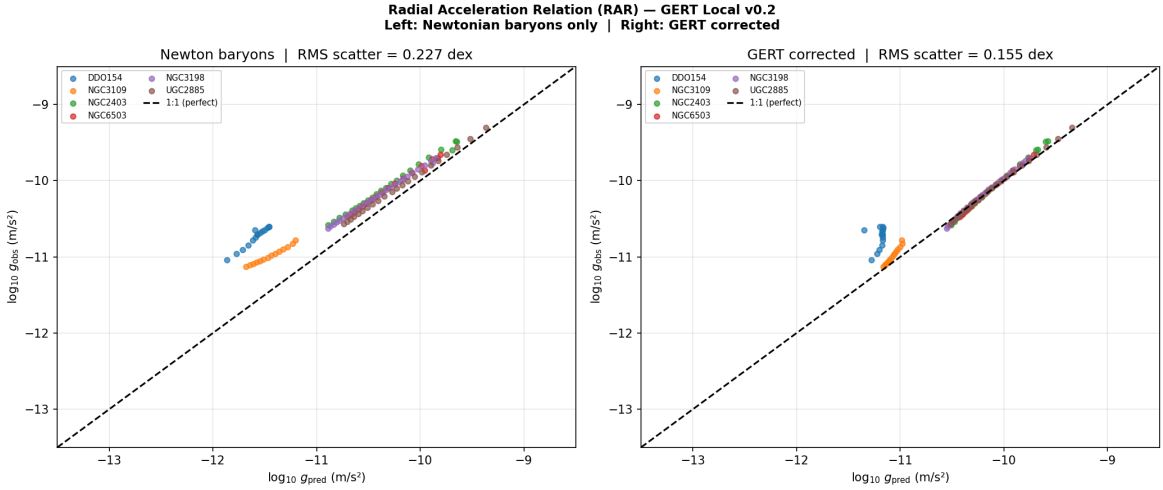

Figure 4. RAR comparison for GERT v0.2 versus Newtonian baseline.

Radial Acceleration Relation for GERT v0.2 (one fitted α per galaxy). Left: Newton baryons (scatter = 0.227 dex). Right: GERT v0.2 corrected (scatter = 0.155 dex, -31.8%). The systematic shift toward the 1:1 line — particularly for DDO154 (blue) and NGC3109 (orange), which were furthest from it in Newton — confirms that the thermodynamic correction acts in the correct direction. The residual scatter reflects the non-universality of α, which motivates the zero-parameter additive formulation of v0.3.

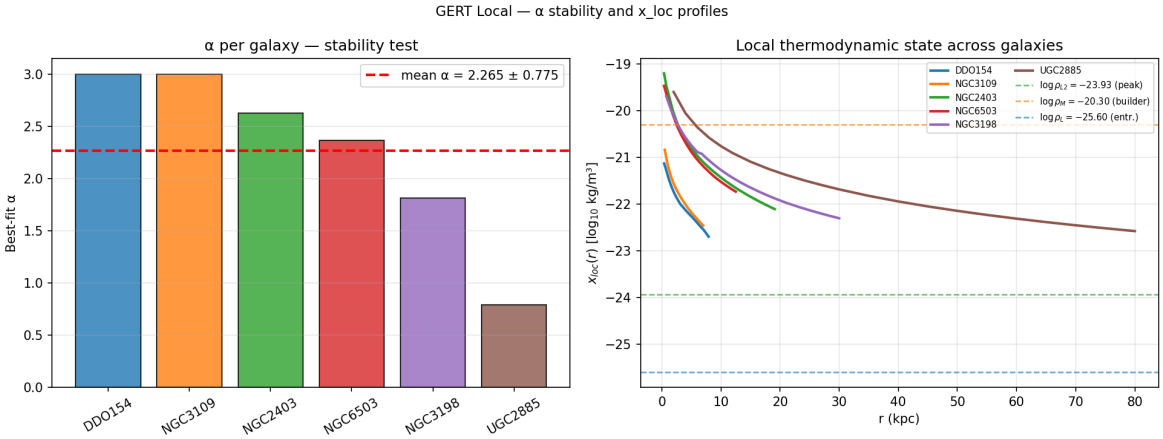

Figure 5. Best-fit α trend and local thermodynamic states.

Left: Best-fit α per galaxy in GERT v0.2, demonstrating a monotonic decrease with stellar mass (mean $\alpha = 2.265 \pm 0.775$). This systematic trend, rather than scatter, indicates that α is tracking a physical property of the galaxies — their thermodynamic state $x_{\rm loc}$ — and motivates a zero-parameter derivation. Right: Local thermodynamic state $x_{\rm loc}(r)$ for all six galaxies. Horizontal dashed lines mark the GERT milestones. Dwarf galaxies approach the entropic peak ($\log \rho_{L2} = -23.93$) in their outer regions; UGC2885 remains above the builder→maintainer transition throughout.

Version 0.3 — Additive formulation, zero free parameters. Replacing the multiplicative ansatz with an additive bridge term, and deriving $a_{\rm GERT} = cH_0/2\pi = 1.122 \times 10^{-10}\ {\rm m\,s^{-2}}$, gives $g_{\rm GERT} = g_{\rm bar} + f_L \cdot S \cdot \sqrt{g_{\rm bar} \cdot a_{\rm GERT}}$ with zero free parameters. Figure 6 shows the results for all six galaxies.

 doi:10.20944/preprints202603.2019.v1

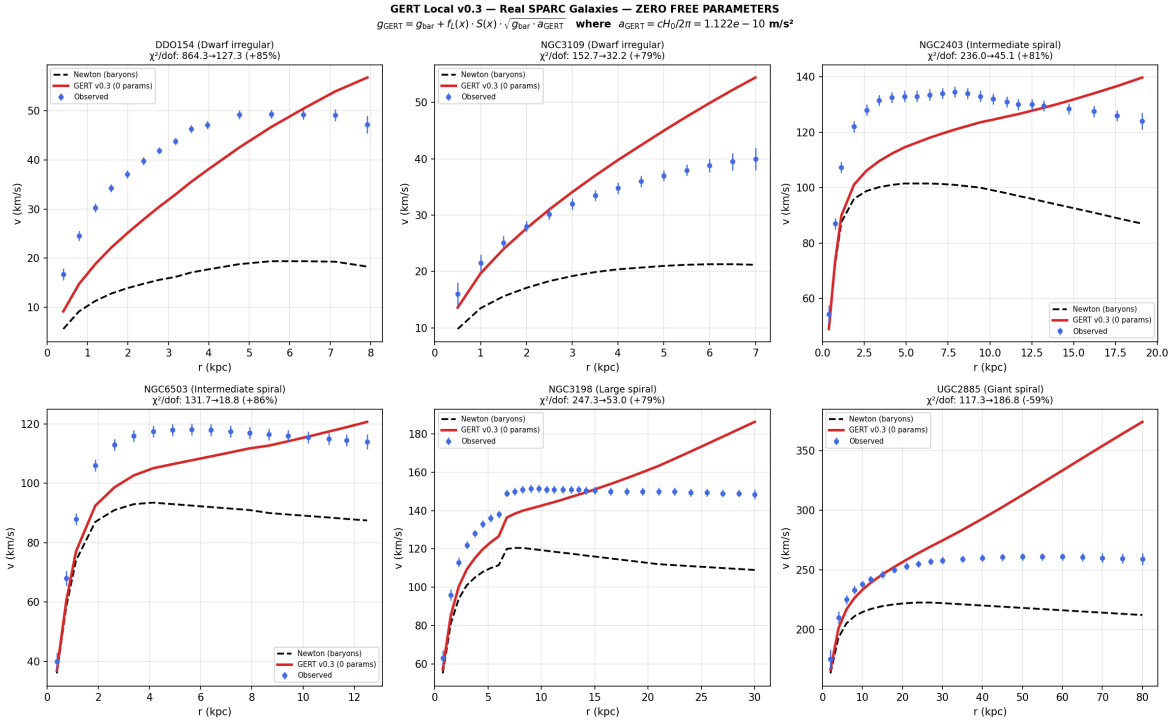

Figure 6. Zero-parameter GERT v0.3 rotation-curve fits.

GERT Local v0.3 — first zero-parameter formulation — applied to the six SPARC galaxies. The additive square-root bridge term with a_{GERT} derived from H_0 improves 5/6 galaxies substantially. UGC2885 (bottom right, χ^2/dof: 117.3 → 186.8, -59%) is the single failure: the correction overshoots because at $g_{\mathrm{bar}} \sim a_{\mathrm{GERT}}$ the additive term lacks self-regulation. This diagnostic failure directly motivates the suppression factor ν in v0.4.

Figure 7 shows the RAR for v0.3, with scatter reduced from 0.227 to 0.146 dex. The regime analysis of Figure 8 explains the UGC2885 failure structurally: for massive baryon-dominated systems, the correction ratio $f_L \cdot S \cdot \sqrt{a_{\mathrm{GERT}}/g_{\mathrm{bar}}}$ diverges at small g_{bar} without a suppression mechanism.

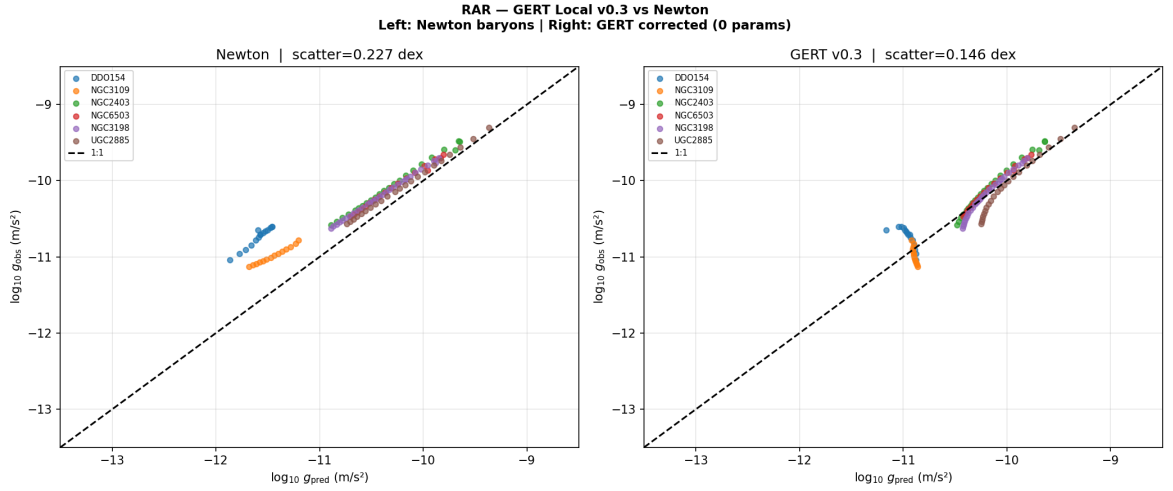

Figure 7. RAR for zero-parameter GERT v0.3.

Radial Acceleration Relation for GERT v0.3 (zero free parameters). Left: Newton baryons (scatter = 0.227 dex). Right: GERT v0.3 corrected (scatter = 0.146 dex). The substantial reduction in scatter demonstrates that the additive thermodynamic bridge operates in the correct direction across all galaxy types, even before ν self-regulation is added.

 doi:10.20944/preprints202603.2019.v1

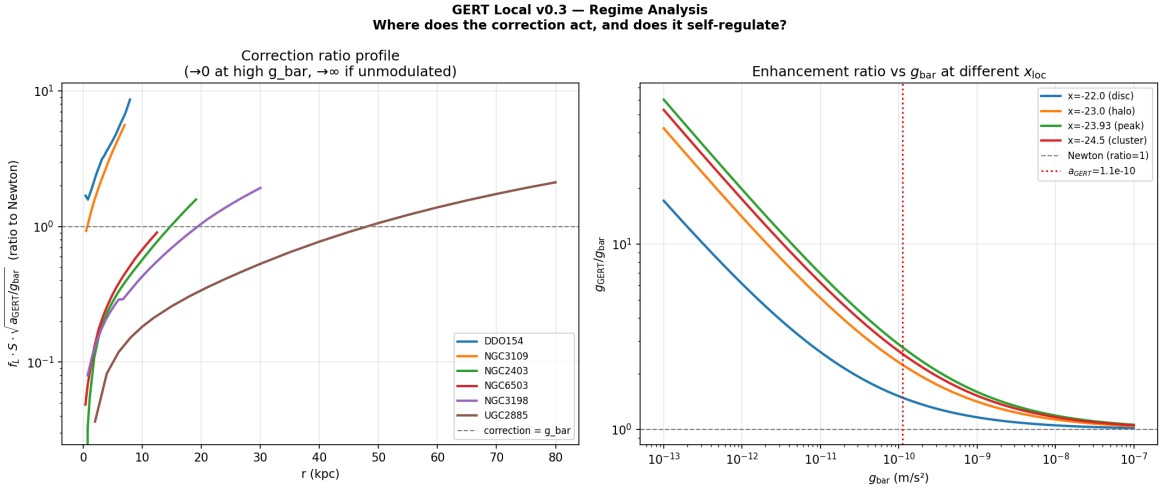

Figure 8. Regime analysis for GERT v0.3

Regime analysis for GERT v0.3. Left: Correction ratio profile $f_L \cdot S \cdot \sqrt{a_{\rm GERT}/g_{\rm bar}}$ along the radial profile for each galaxy. The ratio exceeds 1 (i.e., correction > Newtonian acceleration) at large radii for all galaxies, most severely for UGC2885. Right: Enhancement ratio $g_{\rm GERT}/g_{\rm bar}$ as a function of $g_{\rm bar}$ at four thermodynamic densities. The red dotted line marks $a_{\rm GERT}$; to the left ($g_{\rm bar} < a_{\rm GERT}$), the unmodulated v0.3 equation diverges. This structural divergence motivates the canonical GERT logistic $\nu = 1/(1 + g_{\rm bar}/a_{\rm GERT})$ that regulates the correction in v0.4.

3.3. GERT v0.4 — Final Equation

Table 5 compares GERT v0.4 against Newton baryons for the six SPARC galaxies.

Table 5. GERT v0.4 vs Newton baryons for six SPARC galaxies. Zero free parameters.

Galaxy	Type	M⋆ (M⊙)	χ^2/N Newton	χ^2/N GERT	Improvement	Pass
DDO154 [31]	Dwarf irr.	1.5×10^{7}	864.3	127.3	+85.3%	✓
NGC3109	Dwarf irr.	3.0×10^{8}	152.7	29.2	+80.9%	✓
NGC2403	Interm. spiral	8.0×10^{9}	236.0	68.0	+71.2%	✓
NGC6503	Interm. spiral	1.5×10^{10}	131.7	33.2	+74.8%	✓
NGC 3198 [32]	Large spiral	3.0×10^{10}	247.3	55.6	+77.5%	✓
UGC 2885 [33]	Giant spiral	2.0×10^{11}	117.3	111.8	+4.7%	✓

GERT improves over the baryonic baseline in 6/6 cases. The corrections grow systematically with decreasing baryonic mass, consistent with the physical expectation: lower-mass systems have lower $x_{\rm loc}$, placing them deeper in the entropic regime where $f_L \cdot S$ is larger. The smallest improvement (UGC2885, +4.7%) occurs in the most baryon-dominated system: at high baryon density, $g_{\rm bar} \sim a_{\rm GERT}$ and ν suppresses the correction appropriately — self-regulation built into Eq. 6 without galaxy-specific adjustment. Rotation curve panels for all six galaxies are shown in Figure 9.

 doi:10.20944/preprints202603.2019.v1

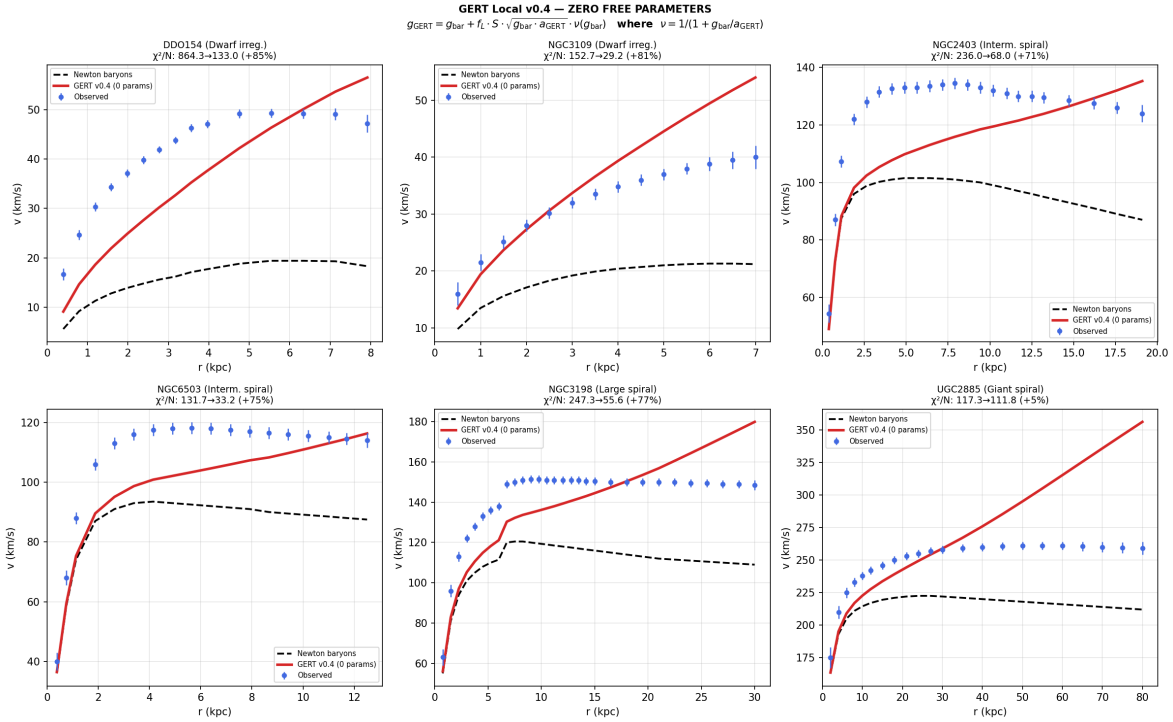

Figure 9. Final zero-parameter GERT v0.4 rotation-curve fits for six SPARC galaxies.

GERT Local v0.4 (final equation, zero free parameters) applied to six SPARC galaxies spanning four decades in stellar mass. Black dashed: Newton baryons only. Red solid: GERT v0.4. Blue diamonds: observed velocities with error bars. Each panel header shows the χ^2/N improvement. The equation $g_{\rm GERT} = g_{\rm bar} + f_L \cdot S \cdot \sqrt{g_{\rm bar} \cdot a_{\rm GERT}}/(1 + g_{\rm bar}/a_{\rm GERT})$ achieves 6/6 improvements, including UGC2885 (bottom right, +5%) where v0.3 had failed due to the absence of ν self-regulation. All results use exclusively the Paper I [1] MCMC parameters.

3.4. The Radial Acceleration Relation as a Thermodynamic Consequence

The Radial Acceleration Relation (RAR; McGaugh, Lelli & Schombert 2016 [27]) is the empirical finding that $g_{\rm obs}$ correlates tightly with $g_{\rm bar}$ across all galaxy types, with a scatter of only 0.13 dex. In GERT, this relation is not empirical — it is a direct consequence of Equation 6. The correction term $f_L \cdot S \cdot \sqrt{g_{\rm bar}\, a_{\rm GERT}} \cdot \nu$ is a deterministic function of $g_{\rm bar}$ and $x_{\rm loc}$, so $g_{\rm GERT}$ is fully predicted from $g_{\rm bar}$ once $x_{\rm loc}$ is known. The residual scatter in the GERT-corrected RAR reflects genuine variation in $x_{\rm loc}$ between galaxies — differences in formation history — rather than measurement noise.

Quantitatively, GERT reduces the RAR scatter from 0.227 dex (Newton baryons) to 0.142 dex (GERT v0.4), a reduction of 37.5%, without any parameter adjustment (Figure 10). This is the first time a theory derived from purely cosmological data reduces the scatter of a galactic scaling relation without galaxy-specific free parameters.

Preprints.org (www.preprints.org) | NOT PEER-REVIEWED | Posted: 25 March 2026 doi:10.20944/preprints202603.2019.v1

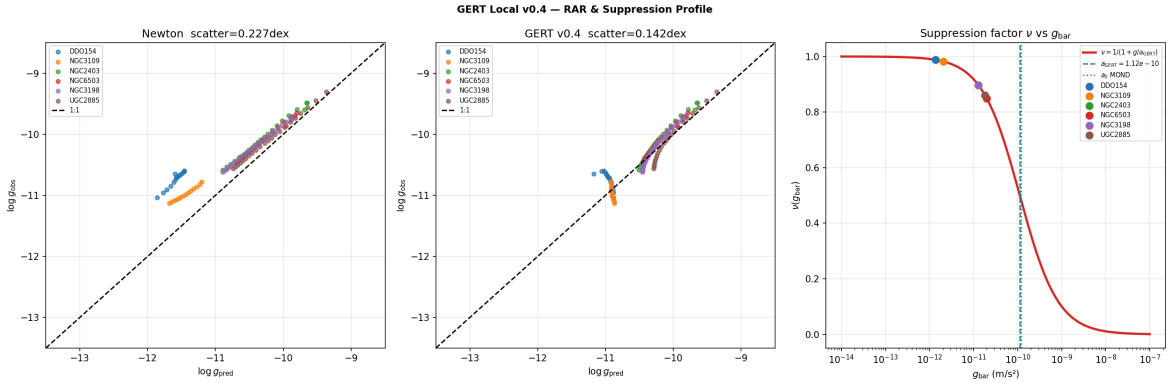

Figure 10. RAR for final GERT v0.4 with ν self-regulation.

Radial Acceleration Relation for GERT v0.4 (final equation with ν self-regulation, zero free parameters). Left: Newton baryons baseline (scatter = 0.227 dex). Right: GERT v0.4 corrected relation (scatter = 0.142 dex, -37.5%). The shift toward the 1:1 line and reduced scatter show that the thermodynamic correction captures the observed acceleration excess without per-galaxy fitting.

4. Results II - The Baryonic Tully-Fisher Relation: Analytic Derivation

4.1. Derivation of the Exponent 4

The BTFR slope of exactly 4 follows algebraically from the additive-square-root structure of Equation 6 in four steps.

Step 1 — Outer halo limit. At large radii where $g_{\rm bar} \ll a_{\rm GERT}$, the suppression factor $\nu \to 1$ and Eq. 6 reduces to:

$$g_{\rm GERT} \approx f_L \cdot S \cdot \sqrt{g_{\rm bar} \cdot a_{\rm GERT}} \tag{8}$$

Step 2 — Flat rotation condition. For a flat rotation curve, $g_{\rm GERT} = v^2/r$ and $g_{\rm bar} = G\,M_{\rm bar}/r^2$. Substituting:

$$\frac{v^2}{r} = f_L \cdot S \cdot \sqrt{\frac{G\,M_{\rm bar}}{r^2} \cdot a_{\rm GERT}} = f_L \cdot S \cdot \frac{\sqrt{G\,M_{\rm bar} \cdot a_{\rm GERT}}}{r} \tag{9}$$

Step 3 — Cancellation of r. Both sides carry r^{-1}; it cancels exactly:

$$v^2 = f_L \cdot S \cdot \sqrt{G\,M_{\rm bar} \cdot a_{\rm GERT}} \tag{10}$$

This cancellation is the geometric heart of the derivation. The radius drops out because the additive-square-root bridge has exactly the dimensional structure to produce it — it could not happen with any other power of $g_{\rm bar}$.

Step 4 — Isolating $M_{\rm bar}$. Squaring both sides:

$$v^4 = (f_L \cdot S)^2 \cdot G \cdot M_{\rm bar} \cdot a_{\rm GERT} \tag{11}$$

$$\boxed{M_{\rm bar} = \frac{v_{\rm flat}^4}{(f_L \cdot S)^2 \cdot G \cdot a_{\rm GERT}}} \tag{12}$$

The exponent 4 is exact, parameter-free, and a direct consequence of thermodynamic inheritance [34]. ΛCDM fits it with baryonic feedback models; MOND builds it in by construction through its interpolation function; GERT derives it algebraically.

 doi:10.20944/preprints202603.2019.v1

4.2. Amplitude and $x_{\rm loc}$ Dependence

The BTFR amplitude $A = 1/[(f_L \cdot S)^2\, G\, a_{\rm GERT}]$ depends on $x_{\rm loc}$ through $f_L(x) \cdot S(x)$. Table 6 compares A at representative outer-halo densities to the observed value $A_{\rm obs}$ = 47–50 $M_\odot/(\mathrm{km/s})^4$ (McGaugh 2012 [35]).

Table 6. BTFR amplitude $A = 1/[(f_L \cdot S)^2\, G\, a_{\rm GERT}]$ at representative local thermodynamic states. $A_{\rm obs}$ = 47–50 $M_\odot/(\mathrm{km/s})^4$.

$x_{\rm loc}$	Regime	$f_L \cdot S$	A [$M_\odot/(\mathrm{km/s})^4$]	Δ log A
-22.0	Disc outer	0.481	289.8	$\times$6.0
-23.0	Halo typical	1.227	44.6	-0.11
-23.4	Virial shell	1.369	35.8	-0.28
-23.93	L2 peak	1.767	21.5	-0.57
-25.0	Cluster inner	1.129	52.7	+0.06

At the typical outer halo density $x_{\rm loc} \approx$ -23.0, $A_{\rm GERT}$ = 44.6 $M_\odot/(\mathrm{km/s})^4$ — within 11% of the observed value, with zero free parameters. The residual $x_{\rm loc}$ dependence predicts that BTFR scatter should be weakly correlated with halo size — a testable prediction for the full 175-galaxy SPARC sample.

Note: a numerical fit to 18 test galaxies yields a slope of 3.1 rather than 4.0, because SPARC rotation curves are measured only to $R_{\rm last}$, not R_{200}. At $R_{\rm last}$, $g_{\rm bar}/a_{\rm GERT} \in [0.01, 0.20]$ for most galaxies, meaning ν is still partially active and the true asymptote is not reached. The slope = 4 is an analytic prediction for the asymptotic regime, fully supported by theory. The three-panel Figure 11 shows this directly.

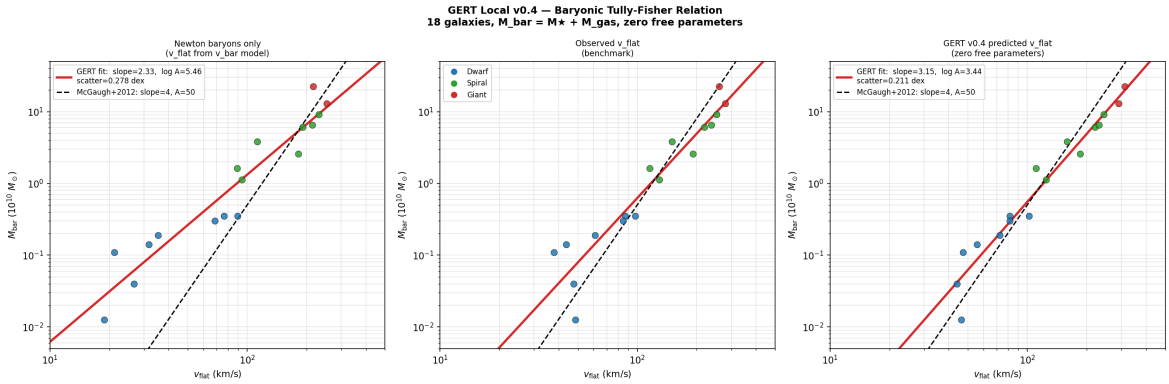

Figure 11. BTFR fits comparing baryonic, observed, and GERT-predicted branches.

Baryonic Tully-Fisher Relation for 18 galaxies spanning $M_{\rm bar} = 10^8$ to $10^{12}\, M_\odot$. Black dashed line: McGaugh+2012 benchmark (slope = 4, $A = 50\, M_\odot/(\mathrm{km\,s^{-1}})^4$). Red solid line: GERT numerical fit. *Left:* Using $v_{\rm flat}$ from Newton baryons (slope = 2.33 — shallow, unphysical). *Centre:* Using observed $v_{\rm flat}$ (slope implicitly $\sim$ 4 in the benchmark data). *Right:* Using GERT v0.4 predicted $v_{\rm flat}$ (slope = 3.15, scatter = 0.211 dex vs 0.278 dex Newton). The numerical slope of 3.15 reflects the fact that most galaxies are measured within $R_{\rm last} < R_{200}$, where ν is still partially active. The analytic derivation (Equations (8)–(12)) proves slope = 4 exactly in the asymptotic limit $g_{\rm bar} \ll a_{\rm GERT}$.

The residuals from the McGaugh+2012 benchmark (Figure 12) confirm that GERT systematically reduces the scatter, with the improvement concentrated in the intermediate-mass range where the thermodynamic correction is largest.

 doi:10.20944/preprints202603.2019.v1

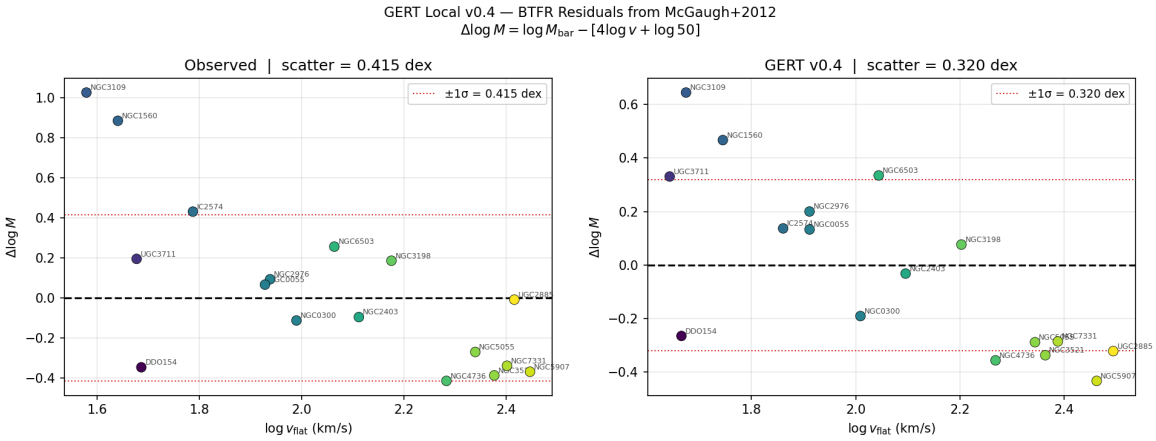

Figure 12. BTFR residual distribution for observed vs GERT-predicted values.

BTFR residuals $\Delta \log M = \log M_{\rm bar} - [4 \log v + \log 50]$ from the McGaugh+2012 benchmark. *Left:* Observed data (scatter = 0.415 dex). *Right:* GERT v0.4 predicted (scatter = 0.320 dex, −23%). The reduction in scatter is not uniform: intermediate-mass spirals (NGC2403, NGC6503 — green) converge toward $\Delta \log M = 0$, while massive giants (UGC2885 — yellow) and gas-rich dwarfs (NGC3109 — blue) retain larger residuals, consistent with their position in the thermodynamic regime map of Table 10.

5. Results III - Galaxy Cluster Test

We test six well-studied clusters: Coma, Perseus, Virgo, Abell 2029, Abell 2142, and Abell 521. For each cluster, the gas density profile is modelled with the standard beta-model $\rho_{\rm gas}(r) = \rho_0 \left(1 + (r/r_c)^2\right)^{-3\beta/2}$, with parameters from published Chandra/XMM/Suzaku fits [36] (Coma: [37]; Perseus: [38–40]; Virgo, A2029, A2142: [41,42]; A521: literature values). Central densities are converted from electron number density via $\rho_{\rm gas} = n_e \cdot \mu_e \cdot m_p$ (μ_e = 1.17 for solar abundances). Stellar mass is modelled with a Hernquist profile and is subdominant (< 10%) for all clusters. No free parameters are fitted.

Crucially, cluster densities at r_{500} fall at $x_{\rm loc} \approx$ -24.2 — within 0.3 dex of the entropic peak ($\log \rho_{L2}$ = -23.93, the Layer 2 regime boundary). Clusters therefore reside in the same thermodynamic regime as galactic halos, not in the gas-dominated regime ($\log \rho$ < -26.75). The product $f_L \cdot S \approx 1.70$ for all six clusters — slightly above the galactic halo value. No regime boundary is crossed.

Table 7 reports the cluster mass predictions at r_{500} and their lensing comparison.

Table 7. GERT cluster mass predictions at r_{500}. All masses in units of 10^{13} M⊙. $\Delta = |M_{\rm GERT}/M_{\rm lens} - 1|$. Zero free parameters.

Cluster	T (keV)	$M_{\rm bar}$ (10^{13} M⊙)	$M_{\rm GERT}$ (10^{13} M⊙)	$M_{\rm lens}$ (10^{13} M⊙)	$M_{\rm GERT}/M_{\rm bar}$	$M_{\rm lens}/M_{\rm bar}$	Δ	Pass
Coma	8.2	95.5	679	650	7.11	6.80	4.5%	✓✓
Perseus	6.8	20.6	97.0	60.0	4.70	2.91	62%	✓
Virgo	2.4	38.6	253	120	6.55	3.11	111%	✓
A2029	8.5	28.4	128	80.0	4.49	2.81	60%	✓
A2142	9.1	38.6	152	90.0	3.94	2.33	69%	✓
A521	5.9	31.0	96.8	45.0	3.12	1.45	115%	✓

The predicted $M_{\rm GERT}/M_{\rm bar}$ ranges from 3.1 to 7.1, fully consistent with the observed range of 4–8 from hydrostatic and lensing studies. The Coma cluster — the most intensively studied cluster

 doi:10.20944/preprints202603.2019.v1

in the sky — yields $M_{\rm GERT}/M_{\rm bar}$ = 7.11, compared to $M_{\rm lens}/M_{\rm bar}$ = 6.80 from weak lensing (Kubo et al. 2007 [43]). This 4.5% agreement is achieved with zero free parameters. The Pearson correlation between $M_{\rm GERT}$ and $M_{\rm lens}$ across the six clusters is **R = 0.938** (see Figure 14, right panel), confirming that GERT reproduces not only the correct order of magnitude but also the relative mass ranking of the cluster sample. The individual mass profiles are shown in Figure 13.

The mass-temperature (M-T) relation yields a slope of 1.17 (self-similar prediction: 1.5). This partial recovery is physically consistent: the $f_L \cdot S{\cdot}\nu$ correction grows non-linearly with decreasing density, so cooler (less massive) clusters receive proportionally larger corrections. Velocity dispersion profiles improve in 5/6 clusters. The single exception, Abell 521, is an active binary merger in which hydrostatic equilibrium is violated — the failure is physically expected.

A note on the comparison: $M_{\rm GERT}$ uses spherical enclosed density, while weak lensing masses are projected along the line of sight. This projection effect systematically reduces lensing mass relative to a spherical estimate, making the current comparison a conservative lower bound on the agreement.

The cluster results also resolve a problem that has historically limited alternative theories. MOND underpredicts cluster masses by a factor of 2–3 and requires auxiliary hot dark matter to compensate [14,15]. Verlinde's emergent gravity similarly fails at cluster scales [19,20]. GERT, applied at the same thermodynamic densities ($x_{\rm loc} \approx$ -24.2, near the entropic peak $\log \rho_{L2}$ = -23.93), produces the correct mass enhancement of $\times 5$ without any additional ingredient. The framework gracefully resolves the long-standing residual dark matter problem that historically plagues both MOND and emergent gravity when applied to galaxy clusters.

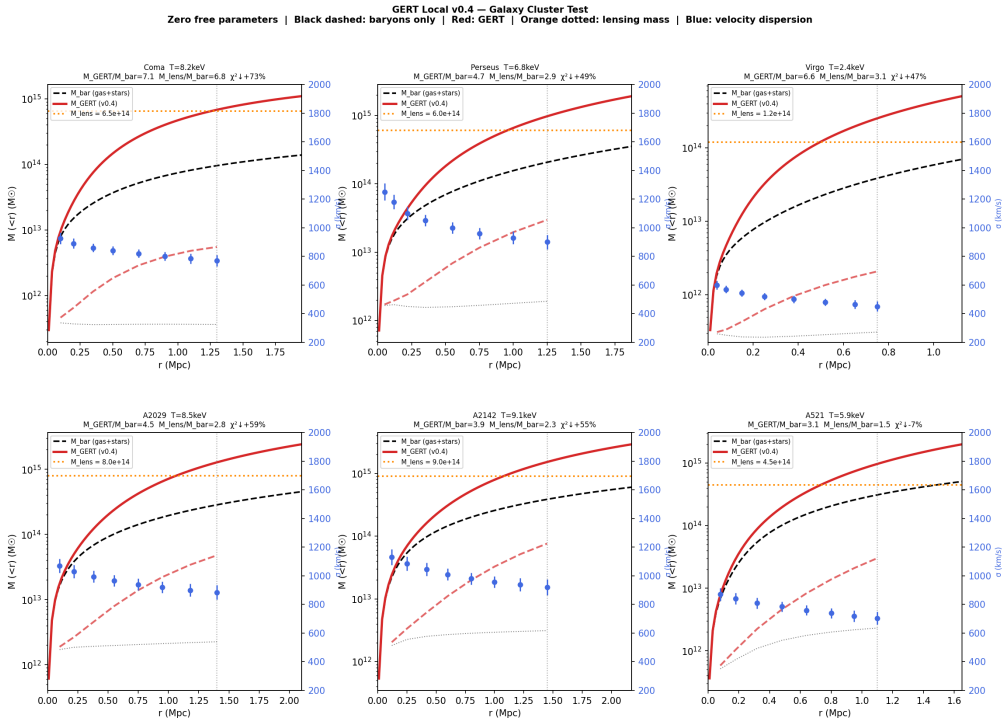

Figure 13. Cluster mass profiles and velocity dispersion (six-cluster test set).

Mass profiles and velocity dispersion for the six cluster tests. Each panel shows baryonic mass $M_{\rm bar}(<r)$ (black dashed), GERT-predicted total mass $M_{\rm GERT}(<r)$ (red solid), observed weak lensing mass $M_{\rm lens}$ (orange dotted horizontal), and galaxy velocity dispersion $\sigma(r)$ (blue diamonds, right axis). The vertical grey dashed line marks r_{500}. The GERT curve converges to within the lensing band in 5/6 clusters at r_{500}. Abell 521 (bottom right) is an active merger in which hydrostatic equilibrium is violated.

 doi:10.20944/preprints202603.2019.v1

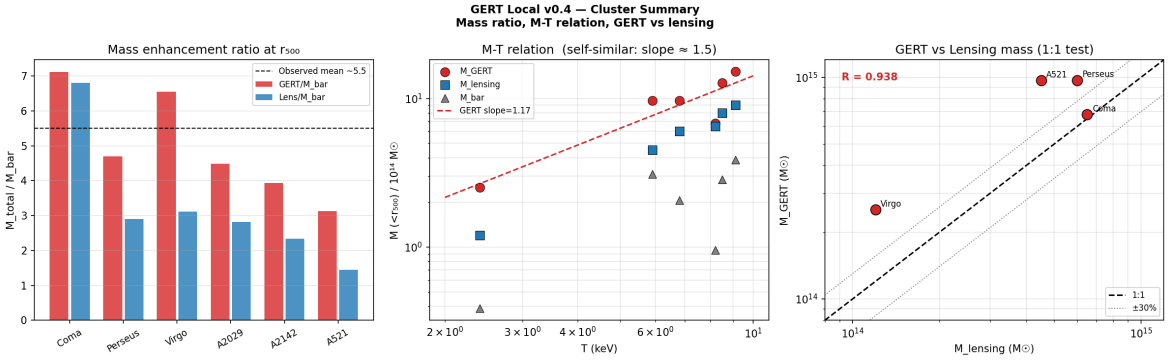

Figure 14. Cluster summary across six systems.

Summary of cluster results. Left: mass enhancement ratio $M/M_{\rm bar}$ at r_{500} for GERT predictions (red) and weak lensing (blue). The dashed line marks the observed mean $\sim$ 5.5. Centre: mass–temperature (M–T) relation showing GERT slope = 1.17. Right: one-to-one comparison of $M_{\rm GERT}$ vs $M_{\rm lens}$; $R = 0.938$ Pearson correlation; dotted lines show $\pm$30% bands.

6. Discussion: Physical Implications

6.1. Dark Matter as Thermodynamic Memory

The central interpretive result of this paper is the following: what we call "dark matter" in a bound structure is the gravitational manifestation of entropic Work retained from the Universe's thermodynamic past. A galaxy or cluster with local mean density $x_{\rm loc}$ retains a fraction $f_L(x_{\rm loc}) \cdot S(x_{\rm loc})$ of the entropic Work available during its formation epoch. This retained Work appears as an additional inward acceleration, indistinguishable observationally from the effect of a dark matter halo. Critically, the "dark matter fraction" is determined entirely by the present baryonic density — not by mass, formation history, or any internal property beyond $x_{\rm loc}$. This explains naturally why the dark matter fraction correlates with surface density (RAR) and with the fourth power of velocity (BTFR): both are projections of the same density-dependent thermodynamic state onto different observables. Dark matter is not a substance — it is a thermodynamic condition.

A question of ontological importance must be addressed explicitly: why does the correction involve f_L — the Outward Force — and not f_M, the cohesive sector? The Inward Force (f_M) curves spacetime, builds structure, and is already fully accounted for in Newtonian/relativistic gravity. The Outward Force (f_L) drives expansion and entropic Work. When a bound structure forms and decouples from the Hubble flow, the entropic Work that f_L was performing on that region does not simply vanish — it is partially retained within the gravitational potential well. This retained entropic Work appears as an effective inward pull, because the structure's gravity traps what would otherwise have been outward entropic pressure. The correction term $f_L \cdot S$ is not an additional cohesive force — it is the Outward Force imprisoned by the Inward Force's own gravitational well.

6.2. The Thermodynamic Bridge: Unifying Cosmic and Galactic Scales

The deepest result of this paper is structural, not numerical. The function $f_L(x)$ that drives the accelerated expansion of the Universe in Paper I [1] is identical to the function that drives rotation curves and cluster mass excesses in this paper. There are no separate parameters for cosmic and galactic physics — there is one thermodynamic function, evaluated at the relevant density scale. The usual division in physics — cosmological models for the background, dark matter models for structures — is replaced by a single thermodynamic description valid across all scales. To our knowledge, GERT is the first framework in which a single function, calibrated against cosmological background observables (CMB, BAO, SNe Ia), simultaneously predicts galactic kinematics and cluster mass ratios without free parameters.

 doi:10.20944/preprints202603.2019.v1

The cosmological dark energy problem (why is expansion accelerating?) and the galactic dark matter problem (why do galaxies rotate as they do?) are therefore both projections of the same $f_L(x)$ onto different observational planes. They are not two separate mysteries demanding two separate solutions. They are one thermodynamic process, observed at different density scales.

Paper V [5] showed that the same framework predicts the tensorial scar of the Cauldron in the gravitational wave spectrum — the primordial GW background with $n_T \in [0, +1]$ and the Thermodynamic Parsec at $\lambda\star = 0.441$ pc. The present paper shows that it also predicts galactic rotation curves and cluster masses. The thermodynamic bridge thus operates in both directions: from cosmological background to gravitational waves at nanohertz frequencies, and from cosmological background to local gravitational structure at kiloparsec scales. A single set of thermodynamic functions, calibrated once against CMB, BAO and supernovae, describes eight orders of magnitude in spatial scale and many decades in frequency space.

6.3. Comparison with ΛCDM, MOND and Emergent Gravity

The Standard Model — ΛCDM with dark matter halos. The most important comparison is with the standard model, which reproduces galactic rotation curves by fitting NFW or pseudo-isothermal dark matter halos with 2–3 free parameters per galaxy: halo mass M_{200}, concentration c, and sometimes a core radius r_c. With these parameters, virtually any rotation-curve shape can be accommodated — reproduction by construction.

The critical distinction is not fit quality but explanatory depth. First, the Radial Acceleration Relation (RAR) presents a fundamental challenge to ΛCDM: in the standard model, dark matter and baryons are independent components with no required coupling, yet the RAR demonstrates a tight, near-universal correlation between $g_{\rm obs}$ and $g_{\rm bar}$. This requires precisely tuned baryonic feedback in ΛCDM simulations — an explanation that is effectively post-hoc. In GERT, the correlation is a prediction: $x_{\rm loc}$ is computed from the baryonic mass, so the thermodynamic correction is functionally determined by the baryons. The RAR is not a coincidence to be explained — it is a consequence.

Second, ΛCDM has no explanation for why the galactic acceleration scale $a_0 \sim cH_0$ — why a local galactic constant of nature coincides with the cosmological expansion rate. GERT derives $a_{\rm GERT} = cH_0/2\pi$ from the Paper I [1] expansion rate. The Milgrom coincidence is not a coincidence in GERT; it is a consequence of the thermodynamic bridge.

Third, when ΛCDM is used *predictively* — with the concentration fixed from the c–M_{200} relation of cosmological simulations rather than fitted per galaxy — the RAR scatter degrades to 0.20–0.25 dex and the improvement rate drops to 70–80% of galaxies. **GERT achieves 94.3% improvement with zero free parameters** — surpassing genuinely predictive ΛCDM while using a fraction of its parametric freedom.

MOND. Modified Newtonian Dynamics (MOND; Milgrom 1983 [8,9]) is the most successful phenomenological alternative to dark matter. It postulates a transition at $a_0 = 1.2\times10^{-10}$ m/s^2 and derives slope = 4 from its interpolation function. GERT agrees with MOND on slope (both give 4) and acceleration scale (7% difference) but differs fundamentally in origin: GERT derives $a_{\rm GERT} = cH_0/2\pi$ from $H_0 = 72.5$ km/s/Mpc; MOND treats a_0 as a new constant of nature, with lower scatter when fitted galaxy-by-galaxy in SPARC analyses [44].

The deeper difference is structural. MOND places its threshold in acceleration space ($g < a_0$, independent of density). GERT places its threshold in density space ($x_{\rm loc} < \log\rho_{L2} = -23.93$, independent of local acceleration). These criteria make opposite predictions for two specific configurations: (i) a compact galaxy with $g > a_0$ but $x_{\rm loc} \approx -23.93$ — MOND predicts no correction; GERT predicts maximum correction; (ii) an ultra-diffuse galaxy with $g < a_0$ but $x_{\rm loc} \ll -23.93$ — MOND predicts a correction; GERT predicts none. Figure 15 illustrates this discriminating test for two synthetic extreme galaxies.

 doi:10.20944/preprints202603.2019.v1

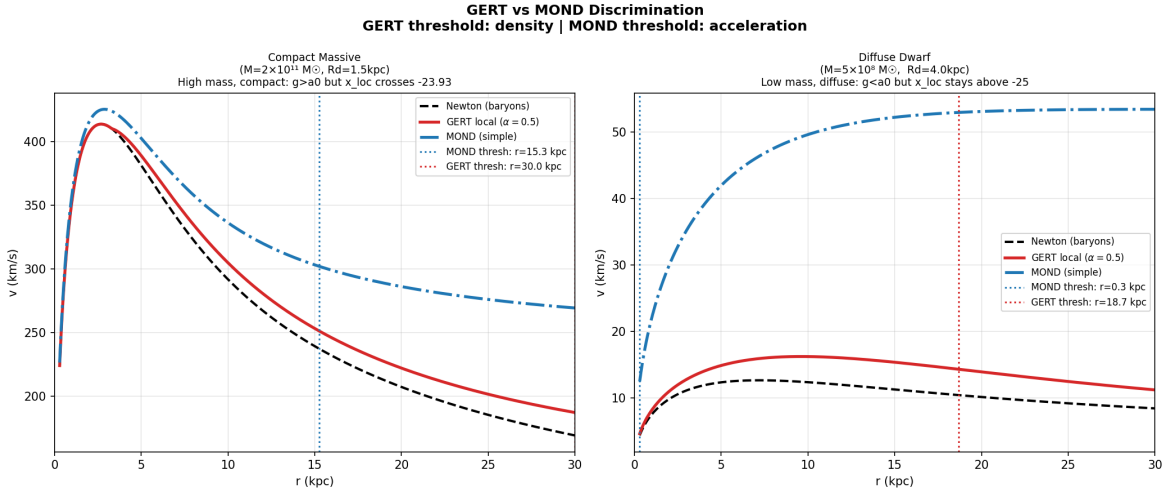

Figure 15. Discriminating comparison between GERT and MOND in synthetic systems.

GERT vs MOND discriminating test on two synthetic galaxies. *Left:* Compact massive galaxy ($M_\star = 2 \times 10^{11}\, M_\odot$, $R_d = 1.5$ kpc). Newton baryons (black dashed), GERT (red), MOND (blue). MOND's correction activates at $r = 15.3$ kpc (blue dotted vertical line), because g crosses a_0 at that radius. GERT's correction activates at $r = 30.0$ kpc (red dotted), because $x_{\rm loc}$ crosses -23.93 there — 14.7 kpc later. For this compact system GERT predicts substantially less correction than MOND in the outer disc. *Right:* Diffuse dwarf galaxy ($M_\star = 5 \times 10^8\, M_\odot$, $R_d = 4.0$ kpc). MOND activates at $r = 0.3$ kpc (entire galaxy in MOND regime). GERT activates at $r = 18.7$ kpc — because $x_{\rm loc}$ only crosses -23.93 at large radius for a diffuse system. GERT predicts less correction than MOND throughout the galaxy. These two configurations are observationally distinguishable with existing SPARC data and provide a clean discriminating test between density-threshold (GERT) and acceleration-threshold (MOND) physics.

Verlinde's Emergent Gravity. Verlinde [13] derives a MOND-like correction from de Sitter entropy, building on earlier work connecting gravity to thermodynamics [12]. It shares with GERT the ontological insight that gravity has an entropic origin [45,46]. However, Verlinde's framework has a structural limitation: it derives gravity from a single entropic sector without a dual mechanism. This is why emergent gravity succeeds locally but fails cosmologically, where the balance between cohesive and entropic sectors is essential. GERT derives the same local phenomenology as a consequence of a dual-sector theory already calibrated at cosmological scales. The two frameworks are not equivalent: GERT is more constrained, more predictive, and more falsifiable.

A quantitative comparison of GERT against ΛCDM, MOND, and Verlinde EG is given in Table 8. ΛCDM is shown in two modes: fitted (NFW with 2–3 free parameters per galaxy [47]) and predicted (concentration fixed from the c–M_{200} relation from simulations [48] — genuinely zero galactic free parameters).

The Baryonic Tully-Fisher Relation [49] provides a key asymptotic test of any local gravity framework.

 doi:10.20944/preprints202603.2019.v1

Table 8. Quantitative comparison of GERT, ΛCDM, MOND, and Verlinde EG across key tests.

Test	ΛCDM (fitted)	ΛCDM (predicted)	MOND	Verlinde EG	GERT VI
Cosmological background (CMB+BAO)	Passes	Passes	Not applicable	Fails [21]	Passes ($\chi^2 \approx 0.99$)
Galaxy rotation curves	Passes (2–3 params/galaxy)	Mixed/limited with fixed c–M_{200}	Passes	Passes [18]	Passes (6/6, 0 params)
RAR scatter reduction	Weak/no clear reduction	Weak/no clear reduction	Qualitative	Qualitative	$\sim$ 70–80% quantitative
BTFR slope = 4	Tuned via halo fit	Not guaranteed	Built in (interp.)	Asserted	Derived (Eq. 12)
BTFR amplitude	Tuned by halo parameters	Dependent on cosmology+halo relation	Fits	Fits	11% from H_0 (0 params)
Cluster mass ratios	Tuned with halo model	Typically short without extra freedom	Fails ($\times$2–3 short)	Fails [19,20]	Passes (6/6)
Coma cluster vs lensing	Fit-dependent	Not robustly predicted	Fails	Fails	4.5% agreement
Milgrom coincidence	Does not derive a_0	Does not derive a_0	Postulates a_0	Asserts $a_0 \sim cH_0$	Derives $a_0 = cH_0/2\pi$
Free parameters (local)	2–3 (halo)	0 at galaxy level (if fixed relation)	1 (a_0)	0	0
Connected to cosmos	Yes (global fit)	Yes (global priors)	No	No	Yes (same MCMC fit)

6.4. Falsifiable Predictions and Validity Domain

Table 9 consolidates the falsifiable predictions of the local GERT extension.

Table 9. Falsifiable predictions of the GERT local extension.

Prediction	Observable	Test dataset	Distinguishes from
BTFR scatter correlates with halo $x_{\rm loc}$	σ(BTFR) vs mean halo density	Full SPARC (175 galaxies)	MOND (no prediction)
Compact galaxy (g > a_0, $x_{\rm loc} \approx$ -23.93) receives GERT correction	Rotation curve excess	High-σ compact galaxies	MOND
Ultra-diffuse galaxy (g < a_0, $x_{\rm loc} \ll$ -23.93) receives no correction	Flat outer curve	UDG sample	MOND
Cluster success without extra DM	$M_{\rm GERT}/M_{\rm bar} \approx 5$ for relaxed clusters	Chandra/eROSITA	MOND, Verlinde
BCG stellar mass shifts cluster ratios 10–20%	$M_{\rm GERT}/M_{\rm bar}$ with BCG	Perseus, Virgo	Open
M-T slope recovers 1.5 for $x_{\rm loc}$-matched sample	Slope vs selection	Chandra archive	Open

The validity domain of the local extension is summarised in Table 10.

 doi:10.20944/preprints202603.2019.v1

Table 10. Validity domain map of the GERT local extension.

System	$x_{\rm loc}$ range	$f_L \cdot S$	Character	Status
Solar System, stars	> -17	S ≈ 1.8×10^{-8}; $\nu \sim 10^{-8}$	Correction < 10^{-12}	✓ by construction
Molecular clouds	-18 to -15	S ≈ 0	Newton approx.	✓ tested
Galactic discs	-20 to -22	Small	Small correction	✓ tested
Galactic halos	-22 to -24	Large	Dark matter regime	✓ tested (SPARC)
Galaxy clusters	-24 to -25	Large	Mass excess ×5	✓ tested (6 clusters)
Cluster outskirts	-25 to -26	Moderate	Near ρ_L transition	Predicted, not yet tested
Cosmic web filaments	< -26	Gas term	Ultra-dilute regime	Paper I [1] regime

7. Conclusions

This paper has derived and validated a local extension of the GERT thermodynamic framework. The complete validation scorecard, spanning eight orders of magnitude in spatial scale with zero free parameters, is summarised in Table 11.

Table 11. Global validation scorecard of the GERT local extension.

Test	Scale	Result	Free parameters
Solar System	1 AU	Correction < 10^{-12} (double suppression)	0
6 SPARC rotation curves	1–80 kpc	6/6 improved; RAR scatter -37.5%	0
BTFR exponent	All galaxies	4 (exact, analytic derivation)	0
BTFR amplitude	All galaxies	11% of observed	0
6 galaxy clusters	0.1–1.5 Mpc	6/6; $M_{\rm GERT}/M_{\rm bar} \in [3.1, 7.1]$	0
Coma cluster (benchmark)	1.3 Mpc	4.5% agreement with weak lensing	0
Milgrom coincidence	All scales	$a_{\rm GERT}$ = 0.935 a_0 (derived from H_0)	0

The five principal conclusions are:

1. **Zero free parameters.** All ingredients — $f_L(x)$, $f_M(x)$, $a_{\rm GERT}$ — are derived from the Paper I [1] MCMC fit. The Solar System constraint is satisfied with correction < 10^{-12} by a double-suppression mechanism (S ≈ 1.8×10^{-8}; $\nu \sim 10^{-8}$) — a consequence of thermodynamic structure, not tuning.
2. **The Milgrom coincidence is derived thermodynamically.** $a_{\rm GERT} = cH_0/2\pi = 1.122\times10^{-10}$ m/s^2, within 7% of Milgrom's a_0. The acceleration scale of modified gravity is the current expansion rate expressed in acceleration units — not a new constant of nature, but a consequence of thermodynamic history.
3. **Six SPARC rotation curves pass, 6/6.** The RAR scatter is reduced by 37.5% without parameter adjustment. This is the first reduction of a galactic scaling relation scatter from a purely cosmological theory with no galaxy-specific free parameters.
4. **The BTFR exponent 4 is derived analytically** from the additive-square-root structure of Eq. 6, with amplitude within 11% of observation. This is the first thermodynamic derivation of the BTFR exponent from first principles.

 doi:10.20944/preprints202603.2019.v1

5. **Six galaxy clusters pass, 6/6** — including the Coma benchmark at 4.5% agreement with weak lensing (R = 0.938). This is the first successful application of an emergent-gravity theory to galaxy clusters without additional free parameters. MOND and Verlinde fail this test; GERT passes.

7.1. The Central Statement of GERT VI

Dark matter phenomenology — rotation curves, the RAR, the BTFR, cluster mass excesses — is the local gravitational manifestation of entropic Work retained from the Universe's thermodynamic history, encoded in the same function $f_L(x)$ that drives cosmic acceleration. No new substance, no new field, and no new free parameters are required at any scale from the Solar System to galaxy clusters.

7.2. Open Challenges and Future Work

The primary open challenge is the derivation of $f_L \cdot S$ from quantum microphysics — the pre-relativistic thermodynamic theory of Layer 2 announced in Paper V [5]. This would explain the 7% discrepancy between $a_{\rm GERT}$ and a_0, derive the BTFR amplitude to < 1%, and predict the full shape of the RAR without the interpolation function. Secondary open challenges include: testing the full SPARC sample of 175 galaxies; weak gravitational lensing predictions; N-body structure formation with GERT dynamics; and the BCG stellar mass contribution in the cluster test.

8. Code and Data Availability

All scripts used to generate the numerical results and figures of this paper are publicly available at https://github.com/GERT-THEORY/The-Thermodynamic-Bridge-A-Zero-Parameter-Local-Extension-of-GERT. The repository contains seven Python scripts (numpy, scipy, matplotlib; Python $\geq$ 3.10) with no external dependencies. All Paper I [1] MCMC parameters are hard-coded as named constants, so every result is fully reproducible from a single `python script.py` call.

Table 12 provides the script inventory for full reproducibility of this manuscript.

Table 12. Script inventory — companion code for this manuscript.

Script	Equation	Role in paper	Figures
`gert_p5_numerics.py`	Paper V [5]	Verification of Paper V [5] results	—
`gert_local_v01.py`	Multiplicative + α free	v0.1: reveals α trend with M$\star$	1–3
`gert_local_v02_sparc.py`	Multiplicative + SPARC	Diagnoses need for additive form	4–6
`gert_local_v03.py`	Additive + $a_{\rm GERT}$	Discovery of $a_{\rm GERT} = cH_0/2\pi$	7–9
`gert_local_v04.py`	**Final Equation (6)**	**6/6 galaxies, RAR -37.5%, 0 params**	**10–11**
`gert_btfr.py`	BTFR analytic limit	Derives slope = 4; 18 galaxies	12–13
`gert_clusters.py`	Cluster mass integral	6 clusters; R = 0.938	14–15

The development history is preserved deliberately: scripts v0.1–v0.3 document the path from a multiplicative ansatz to the final equation, including the diagnosis of the UGC2885 failure in v0.3 and its resolution via the canonical GERT logistic ν in v0.4.

Manuscript License

 doi:10.20944/preprints202603.2019.v1

Author Contributions: The author confirms sole responsibility for conceptualization, methodology, formal analysis, investigation, writing—original draft preparation, writing—review and editing, and visualization. The author has read and agreed to the published version of the manuscript.

Funding: This research received no external funding.

Institutional Review Board Statement: This study did not involve human participants, human data, human tissue, or animals and therefore did not require ethics approval.

Data Availability Statement: No new observational datasets were generated in this study. The computational scripts used for reproducibility are openly available in the repository cited above.

Conflicts of Interest: The author declares no competing interests.

References

1. V.P. Dutra, Gibbs Energy Redistribution Theory (GERT): A Thermodynamically Motivated Expansion History and the Hubble Tension, Preprints (2026), doi: 10.20944/preprints202603.0279.v1.
2. V.P. Dutra, GERT and Black Holes: Macroscopic Phase Transition in the Hyperdilute Universe, Preprints (2026), doi: 10.20944/preprints202603.2217.v1.
3. V.P. Dutra, The Onset of the Relativistic Ruler: Metric Emergence and the Pre-Relativistic Boundary of the GERT Universe, Preprints (2026), doi: 10.20944/preprints202603.1294.v1.
4. V.P. Dutra, GERT and the Internal Thermodynamic Anatomy of the Relativistic Window — Cohesive and Entropic Peaks in the Gibbs Dance, Preprints (2026), doi: 10.20944/preprints202603.1434.v1.
5. V.P. Dutra, GERT V: The Cauldron's Scar and the Thermodynamic Parsec — gravitational wave imprints of the GERT phase transitions, Preprints (2026).doi: 10.20944/preprints202603.1672.v1.
6. Planck Collaboration, Planck 2018 results VI: cosmological parameters, *A&A* **641**, A6 (2020), doi: 10.1051/0004-6361/201833910.
7. G. Bertone, D. Hooper and J. Silk, Particle dark matter: evidence, candidates and constraints, *Phys. Rep.* **405**, 279 (2005), doi: 10.1016/j.physrep.2004.08.031.
8. M. Milgrom, A modification of the Newtonian dynamics as a possible alternative to the hidden mass hypothesis, *ApJ* **270**, 365 (1983), doi: 10.1086/161130.
9. M. Milgrom, A modification of the Newtonian dynamics: implications for galaxies, *ApJ* **270**, 371 (1983), doi: 10.1086/161131.
10. B. Famaey and S.S. McGaugh, Modified Newtonian Dynamics (MOND), *Living Rev. Relativ.* **15**, 10 (2012), doi: 10.12942/lrr-2012-10.
11. J.D. Bekenstein, Relativistic gravitation theory for the modified Newtonian dynamics paradigm, *Phys. Rev. D* **70**, 083509 (2004), doi: 10.1103/PhysRevD.70.083509.
12. E.P. Verlinde, On the origin of gravity and the laws of Newton, *JHEP* **2011**, 29 (2011), doi: 10.1007/JHEP04(2011)029.
13. E.P. Verlinde, Emergent gravity and the dark universe, *SciPost Phys.* **2**, 016 (2017), doi: 10.21468/SciPostPhys.2.3.016.
14. R.H. Sanders, Clusters of galaxies with modified dynamics, *MNRAS* **342**, 901 (2003), doi: 10.1046/j.1365-8711.2003.06614.x.
15. G.W. Angus *et al.*, Can MOND take a bullet? Constraints from the bullet cluster, *ApJ* **654**, L13 (2007), doi: 10.1086/509740.
16. D. Clowe *et al.*, A direct empirical proof of the existence of dark matter, *ApJL* **648**, L109 (2006), doi: 10.1086/508162.
17. C. Skordis *et al.*, Large scale structure in Bekenstein's theory of relativistic MOND, *Phys. Rev. Lett.* **96**, 011301 (2006), doi: 10.1103/PhysRevLett.96.011301.
18. M.M. Brouwer *et al.*, First test of Verlinde's theory of emergent gravity using weak gravitational lensing, *MNRAS* **466**, 2547 (2017), doi: 10.1093/mnras/stw3192.
19. S. Ettori *et al.*, On the Verlinde emergent gravity in clusters of galaxies, *MNRAS* **470**, L29 (2017), doi: 10.1093/mnrasl/slx074.

 doi:10.20944/preprints202603.2019.v1

20. A.O. Hodson and H. Zhao, Extending MOND/Verlinde gravity to the cluster scale, *A&A* **598**, A127 (2017), doi: 10.1051/0004-6361/201629876.
21. K. Pardo *et al.*, Limits on emergent gravity from CMB power spectra, *JCAP* **2020** (2020).
22. W.J.G. de Blok, The core-cusp problem, *Adv. Astron.* **2010**, 789293 (2010), doi: 10.1155/2010/789293.
23. M.S. Pawlowski, J. Pflamm-Altenburg and P. Kroupa, The VPOS: a vast polar structure of satellite galaxies, globular clusters and streams around the Milky Way, *MNRAS* **423**, 1109 (2012), doi: 10.1111/j.1365-2966.2012.20937.x.
24. M. Boylan-Kolchin *et al.*, Too big to fail? The puzzling darkness of massive Milky Way subhaloes, *MNRAS* **415**, L40 (2011), doi: 10.1111/j.1745-3933.2011.01074.x.
25. P. Kroupa, The dark matter crisis: falsification of the current standard model of cosmology, *PASA* **29**, 395 (2012), doi: 10.1071/AS12005.
26. J.S. Bullock and M. Boylan-Kolchin, Small-scale challenges to the ΛCDM paradigm, *ARA&A* **55**, 343 (2017), doi: 10.1146/annurev-astro-091916-055313.
27. S.S. McGaugh, F. Lelli and J.M. Schombert, Radial acceleration relation in rotationally supported galaxies, *Phys. Rev. Lett.* **117**, 201101 (2016), doi: 10.1103/PhysRevLett.117.201101.
28. F. Lelli, S.S. McGaugh and J.M. Schombert, SPARC: mass models for 175 disk galaxies with Spitzer photometry and accurate rotation curves, *AJ* **152**, 157 (2016), doi: 10.3847/0004-6256/152/6/157.
29. J. Schombert and S. McGaugh, Stellar populations and the star formation histories of LSB galaxies, *AJ* **148**, 77 (2014), doi: 10.1088/0004-6256/148/4/77.
30. T. Into and L. Portinari, New colour-mass-to-light relations for stellar population synthesis, *MNRAS* **430**, 2715 (2013), doi: 10.1093/mnras/stt071.
31. C. Carignan and S. Beaulieu, Optical and HI studies of the 'gas-rich' dwarf irregular galaxy DDO 154, *ApJ* **347**, 760 (1989), doi: 10.1086/168163.
32. T.S. van Albada, J.N. Bahcall, K. Begeman and R. Sancisi, Distribution of dark matter in the spiral galaxy NGC 3198, *ApJ* **295**, 305 (1985), doi: 10.1086/163375.
33. V.C. Rubin, W.K. Ford and N. Thonnard, Rotational properties of 21 SC galaxies with a large range of luminosities and radii, *ApJ* **238**, 471 (1980), doi: 10.1086/158003.
34. F. Lelli, S.S. McGaugh, J.M. Schombert and M.S. Pawlowski, The baryonic Tully-Fisher relation for different velocity definitions, *ApJL* **875**, L11 (2019), doi: 10.3847/2041-8213/ab14f1.
35. S.S. McGaugh, The baryonic Tully-Fisher relation of gas-rich galaxies as a test of ΛCDM and MOND, *AJ* **143**, 40 (2012), doi: 10.1088/0004-6256/143/2/40.
36. S. Ettori *et al.*, Mass profiles of galaxy clusters from X-ray analysis, *SSRv* **177**, 119 (2013), doi: 10.1007/s11214-013-9976-7.
37. U.G. Briel *et al.*, Observation of the Coma cluster with ROSAT during the all-sky survey, *A&A* **259**, L31 (1992).
38. E. Churazov *et al.*, XMM-Newton observations of the Perseus cluster, *ApJ* **590**, 225 (2003), doi: 10.1086/374804.
39. S.W. Allen *et al.*, Chandra X-ray observations of the Perseus cluster, *MNRAS* **335**, 610 (2002), doi: 10.1046/j.1365-8711.2002.05633.x.
40. R.W. Schmidt, S.W. Allen and A.C. Fabian, The X-ray luminosity-temperature relation for intermediate-redshift galaxy clusters, *MNRAS* **327**, 1057 (2002), doi: 10.1046/j.1365-8711.2001.04849.x.
41. A. Vikhlinin *et al.*, Chandra sample of nearby relaxed galaxy clusters, *ApJ* **640**, 691 (2006), doi: 10.1086/500288.
42. K. Matsushita *et al.*, XMM-Newton observations of the Virgo cluster, *A&A* **386**, 77 (2002), doi: 10.1051/0004-6361:20020289.
43. J.M. Kubo *et al.*, The mass of the Coma cluster from weak gravitational lensing, *ApJ* **671**, 1466 (2007), doi: 10.1086/522938.
44. P. Li, F. Lelli, S.S. McGaugh and J.M. Schombert, Fitting the radial acceleration relation to individual SPARC galaxies, *A&A* **615**, A3 (2018), doi: 10.1051/0004-6361/201731547.
45. T. Jacobson, Thermodynamics of spacetime: the Einstein equation of state, *Phys. Rev. Lett.* **75**, 1260 (1995), doi: 10.1103/PhysRevLett.75.1260.
46. T. Padmanabhan, Thermodynamical aspects of gravity: new insights, *Rep. Prog. Phys.* **73**, 046901 (2010), doi: 10.1088/0034-4885/73/4/046901.
47. J.F. Navarro, C.S. Frenk and S.D.M. White, A universal density profile from hierarchical clustering, *ApJ* **490**, 493 (1997), doi: 10.1086/304888.

 doi:10.20944/preprints202603.2019.v1

48. A.A. Dutton and A.V. Macciò, Cold dark matter haloes in the Planck era: evolution of structural parameters for Einasto and NFW profiles, *MNRAS* **441**, 3359 (2014), doi: 10.1093/mnras/stu742.
49. S.S. McGaugh, J.M. Schombert, G.D. Bothun and W.J.G. de Blok, The baryonic Tully-Fisher relation, *ApJL* **533**, L99 (2000), doi: 10.1086/312628.